Universidade Federal do Rio de Janeiro
Escola Politécnica

CALIBRATION OF DEM CONTACT PARAMETERS FOR TUMBLING MILLS USING PEPT

Anderson Silva das Chagas

Projeto de Graduação apresentado ao Curso de Engenharia Metalúrgica da Escola Politécnica, Universidade Federal do Rio de Janeiro, como parte dos requisitos necessários à obtenção do título de Engenheiro Metalúrgico.

Orientador: Prof. Luís Marcelo Marques Tavares

Coorientador: Prof. Rodrigo Magalhães de Carvalho

Rio de Janeiro

Novembro de 2015

CALIBRATION OF DEM CONTACT PARAMETERS FOR TUMBLING MILLS USING PEPT

Anderson Silva das Chagas

PROJETO DE GRADUAÇÃO SUBMETIDO AO CORPO DOCENTE DO CURSO DE ENGENHARIA METALÚRGICA DA ESCOLA POLITÉCNICA DA UNIVERSIDADE FEDERAL DO RIO DE JANEIRO COMO PARTE DOS REQUISITOS NECESSÁRIOS PARA A OBTENÇÃO DO GRAU DE ENGENHEIRO METALÚRGICO.

Examinado por:

Prof. Luís Marcelo Marques Tavares, PhD.

Prof. Rodrigo Magalhães de Carvalho, DSc.

Profa. Gabriela Ribeiro Pereira, DSc.

Prof. Aubrey Njema Mainza, PhD.

RIO DE JANEIRO, RJ – BRASIL

Novembro de 2015

Chagas, Anderson Silva

Calibration of DEM contact parameters for tumbling mills using PEPT/ Anderson Silva das Chagas. – Rio de Janeiro: UFRJ/ Escola Politécnica, 2015.

XVIII, 64, p.: il.; 29,7 cm.

Orientador: Luís Marcelo Marques Tavares

Coorientador: Rodrigo Magalhães de Carvalho

Projeto de Graduação – UFRJ/ Escola Politécnica/ Curso de Engenharia Metalúrgica, 2015.

Referências Bibliográficas: p. 62-65.

1. Comminution. 2. Energy efficiency. 3. Ball milling. I. Tavares, Luís Marcelo Marques e Carvalho, Rodrigo Magalhães de. II. Universidade Federal do Rio de Janeiro, Escola Politécnica, Curso de Engenharia Metalúrgica. III. Calibration of DEM contact parameters for tumbling mills using PEPT.

"*The only place success comes before work is in the dictionary*"

Vince Lombardi

Acknowledgments

I would like to thank the following persons for their contribution to this work:

- Professor Luis Marcelo Tavares, to whom I am grateful for the guidance over the years and the confidence entrusted on me. More than advisor, a model of professional to be followed.
- Professor and colleague Rodrigo Carvalho, for countless hours of advisory and patience in guiding me through this journey.
- LTM team, for their support, incredible knowledge exchange and for the laughs.
- Professors Aubrey Mainza and Lawrence Bbosa, for welcoming into their work group, their invaluable encouragement and enduring advices.
- And last but not least, my lovely wife, for incredible patience and belief throughout the years.

Resumo do Projeto de Graduação apresentado à Escola Politécnica/ UFRJ como parte dos requisitos necessários para obtenção do grau de Engenheiro Metalúrgico.

CALIBRATION OF DEM CONTACT PARAMETERS FOR TUMBLING MILL USING PEPT

Anderson Silva das Chagas

Novembro/ 2015

Orientador: Luís Marcelo Marques Tavares

Coorientador: Rodrigo Magalhães de Carvalho

Curso: Engenharia Metalúrgica

Moinhos de tubulares estão entre os equipamentos mais utilizados na cominuição de minerais, apresentando grande robustez, e sendo capaz de lidar com grandes quantidades de material por dia em uma ampla faixa de tamanhos de partículas. Embora moinhos tubulares tenham sido desenvolvidos para um elevado grau de confiabilidade mecânica, eles são extremamente ineficientes em termos de energia cosumida. A modelagem e completa compreensão do comportamento e mecanismos relacionados a quebra de partículas em moinhos tubulares são de extrema importância. Entretanto, a compreensão do ambiente mecânico no interior de moinhos durante sua operação apresenta certos desafios uma vez que moinhos tubulares são sistemas fechados e opacos, tornando a completa quantificação da distribuição de carga e seu movimento extremamente difícil ou mesmo impossível.

O Método de elementos discretos (DEM) é altamente adequado para o problema dos moinho tubulares e consiste em aplicar as leis de movimento de Newton a corpos particulados em movimento e um modelo de forças de deslocamento aos corpos em colisão. A fim de que a simulação de DEM possa descrever o movimento de partículas com fidelidade ao equipamento real é necessário o uso de parâmetros de materiais e de contato adequados. Esses parâmetros podem ser estimados por meio de calibração, através comparação quantitativa de resultados experimentais e simulação. Neste sentido, é vantajosa a utilização de moinhos de escala de laboratório.

O Rastreamento de partículas per emissão positrônica (PEPT) é uma técnica para a medição da trajetória de uma partícula traçador radioativo em um sistema granular ou fluido, tal qual um moinho tubular e apresenta-se como uma técnica ideal para, em alguns casos, a calibração de parâmetros DEM.

O principal objetivo do presente trabalho é sugerir uma metodologia para a calibração de parâmetros de contato, para simulações DEM, usando dados adquiridos a partir de testes em um moinho de laboratório usando a técnica PEPT. Algumas opções de comparação entre PEPT e DEM são apresentadas e a validade da própria comparação é avaliada.

Palavras-chave: Método de elementos discretos, Positron Emission Particle Tracking, Moagem, Parâmetros de contato.

Abstract of Undergraduate Project presented to POLI/UFRJ as a partial fulfillment of the requirements for degree of Metallurgical Engineer.

CALIBRATION OF DEM CONTACT PARAMETERS FOR TUMBLING MILL USING PEPT

Anderson Silva das Chagas

November/ 2015

Advisors: Luís Marcelo Marques Tavares

Rodrigo Magalhães de Carvalho

Course: Metallurgical Engineering (BEng)

Tumbling mills are among the most used equipments in the comminution of minerals, presenting great robustness, and being capable of dealing with large tonnages of material per day and a wide size range for the feed. Although tumbling mills have been developed to a high degree of mechanical efficiency and reliability, they are extremely wasteful in terms of energy expended. The modeling and complete understanding of the charge behavior and mechanisms related to particle breakage in tumbling mills are of extreme importance. However, understanding the mechanical environment inside the mill during operation presents certain challenges since tumbling mills are closed and opaque systems, making the complete quantification of charge distribution and motion extremely difficult or even impossible.

The discrete element method (DEM) is highly suitable for the tumbling mill problem and consists of applying Newton's second law to particulate bodies in motion and a force displacement model to the bodies in collision. In order for a DEM simulation to describe the particle movement with fidelity to the real equipment, it is necessary to use proper material and contact parameters. Those parameters can be estimated through calibration, by quantitative comparison of experimental and simulation results. In that sense, it is advantageous to use laboratory-scale mills.

The Positron Emission Particle Tracking (PEPT) is a technique for measuring the flow trajectory of a radioactive particle tracer in a granular or fluid system such as a

tumbling mill and presents itself as an ideal technique for calibrating DEM parameters in some cases.

The main objective of the present work is to suggest a methodology for the calibration of contact parameters, for DEM simulations, using data acquired from tests in a mill using the PEPT technique. Some options of comparing PEPT and DEM are presented and the validity of the comparison itself is assessed.

Keywords: Discrete Element Method, Positron Emission Particle Tracking, Mills, Contact Parameters

Table of Contents

Acknowledgments v

List of Figures xi

List of Tables xiv

Nomenclature xv

1. Introduction 1

2. Objective 4

3. Review of the literature 5

3.1. Grinding 5

3.2. Discrete Element Method (DEM) 11

3.3. Positron Emission Particle Tracking (PEPT) 18

4. Materials and methods 24

4.1. PEPT charge motion experiments 24

4.2. Processing of the PEPT data 26

4.3. DEM simulations 30

4.4. Calibration methodology 32

5. Results and discussion 34

5.1. PEPT experiments results 34

5.2. Validation of ergodic hypothesis 40

5.3. DEM parameters calibration 43

5.3.1. Preliminary design of DEM simulations experiments 43

5.3.2. Refined design of DEM simulation experiments 47

5.4. DEM parameters calibration 53

6. Conclusions 57

7. Future work 59

8. References 60

List of Figures

Figure 3. 1 – Types of stress mechanisms inside grinding equipment. Larger circles representing grinding media and smaller circles representing ore particles..... 5

Figure 3. 2 – Charge motion inside a mill: a) cascade; b) cataract; c) centrifugal. 7

Figure 3. 3 – Charge features. 7

Figure 3. 4 – Influence of fraction of the critical speed on power consumption (Kelly and Spottiswood 1982). 9

Figure 3. 5 – Mill charge scheme according to Morrell (1996). 10

Figure 3. 6 – DEM simulation of the effect of liner design in a 0.6 m diameter mill operating at 68% of critical speed, with 30% ball filling and 25 mm steel balls (Carvalho & Tavares 2013). 11

Figure 3. 7 – Effect of the coefficient of friction on mill power draw (van Nierop et al. 2001). 15

Figure 3. 8 – Experimental setup used for validation of DEM simulation by Pérez-Alonso and Delgadillo (Pérez-Alonso & Delgadillo 2012). 16

Figure 3. 9 – Tumbling mills fitted with inductive proximity probe (Kiangi et al. 2013).. 17

Figure 3. 10 – Photograph of biplanar X-ray imaging system (Govender et al. 2001).. 17

Figure 3. 11 – Laboratory scale tumbling mill in PET camera and schematic of the triangulation. 19

Figure 3. 12 – Spatial distribution of porosity at different mill speeds, with a Rosin-Rammler distribution of glass beads at discrete sizes of 2-8 mm in a 300 mm diameter mill (Sichalwe et al. 2011). 20

Figure 3. 13 – Diagram illustrating power draw calculation..... 21

Figure 3. 14 – Spatial plot of the power draw distribution in Watts at 60% of critical speed, for 31.3% mill filling of monosize 3 mm glass beads in a 300 mm diameter mill (Bbosa et al. 2011). 22

Figure 3. 15 – Absolute velocity and porosity plots for PEPT and DEM at 75% of critical speed, for 31.3% mill filling of monosize 5 mm glass beads in a 300 mm diameter mill (Govender et al. 2013). 23

Figure 4. 1 – Tumbling mill settings and internal schematic. 25

Figure 4. 2 – Tracer's vertical coordinate parameterized with respect to time (a) and interpolated trajectory (b). 27

Figure 4. 3 – Tracer's position along the mill length over time. 27

Figure 4. 4 – PEPT tracer's coordinates (a) and interpolated trajectory (b) at 60% of the critical speed. 28

Figure 4. 5 – PEPT tracer's coordinates (a) and interpolated at 60% of the critical speed. 29

Figure 4. 6 – PEPT tracer's coordinates (a) and interpolated at 60% of the critical speed. 29

Figure 4. 7 – Diagram illustrating power draw calculation.**Erro! Indicador não definido.**

Figure 4. 8 – Snapshot of a DEM simulation at 60% critical mill speed. 31

Figure 4. 9 – Power draw predicted over time for DEM simulation at 60% c.s. 32

Figure 5. 1 – Superposition of the tracer's coordinates for 50, 60 and 75% critical speed. 34

Figure 5. 2 – Spatial plots of location probability (left) and absolute velocity [m/s] (right) for 50, 60 and 75% critical speed. 36

Figure 5. 3 – Particle distributions in X and Y directions. 37

Figure 5. 4 – Distributions of velocity normalized by mill speed for PEPT data. 37

Figure 5. 5 – Comparison between power draw that was measured and estimated from PEPT. 38

Figure 5. 6 – Spatial power draw distribution [W] for 50, 60 and 75% of mill critical speed. 39

Figure 5. 7 – Spatial absolute velocity [m/s] (left) and power draw [W] (right) for the single particles and for the whole charge. 41

Figure 5. 8 – Comparison of the particle and velocity distribution of a single particle treated as PEPT, and the mill charge, at 60% critical speed. 42

Figure 5. 9 – Objective function values for the preliminary design of DEM simulation experiments, conducted at 75% critical speed. 44

Figure 5. 10 – Power draw calculated for PEPT and DEM simulations in the preliminary design of simulation experiments. 45

Figure 5.11 – Influence of the coefficient of friction on the power draw. Extracted from van Nierop et al. (2001), at 80% critical speed with 35% mill filling (dashed line) and the analysis done for the PEPT mill system, at 75% critical speed (full line). 46

Figure 5. 13 – Objective function values for the refined design of DEM simulation experiments, for the mill operating at 75% critical speed. 49

Figure 5. 14 – Response surface of the objective function in relation to the parameters CFPP and CRPG. 50

Figure 5. 15 – Spatial power distribution [W] for (a) PEPT, (b) DEM with calibrated parameters and (c) difference PEPT - DEM. 52

Figure 5. 16 – Power draw measured and calculated using PEPT and DEM simulations with the calibrated parameters at 75% critical speed. 52

Figure 5. 17 – Distributions of (a) particle in the horizontal direction, of (b) velocity and their cumulative frequency (c and d), at 75% critical speed. 53

Figure 5. 18 – Power draw calculated using PEPT data and DEM simulations with the calibrated parameters. 54

Figure 5. 19 – Particle distributions in X direction for PEPT and DEM simulations with the calibrated parameters. 55

List of Tables

Table 3. 1 – Summary of charge definitions. 8

Table 4. 1 – Material parameters for DEM simulations. 30

Table 4. 2 – Summary of calibrated contact parameters 33

Table 5. 1 – Power draw [W] calculated for the whole charge of particles and for the single particles. 42

Table 5. 2 – Preliminary fractional factorial design of DEM simulation experiments along with the calculated power draw and the objective function (OF) value. 43

Table 5. 3 – Analysis of variance (ANOVA) for the preliminary design of simulation experiments, where DF is the number of degrees of freedom, SS the sum of squares and MS the mean squares. 46

Table 5. 4 – Central composite design of DEM simulation for the CFPP and CRPG along with the calculated power draw and the objective function (OF) value. 48

Table 5. 5 – Analysis of variance (ANOVA) for the second design of simulation experiments. 49

Table 5. 6 – Optimal set of contact parameters. 50

Nomenclature

CFD	Computational Fluid Dynamics
DEM	Discrete Element Method
FEM	Finite Element Method
HDPE	High Density Polyethylene
PEPT	Positron Emission Particle Tracking
PET	Positron Emission Tomography
SAG	Semi-autogenous grinding
SPH	Smoothed Particles Hydrodynamics
UCT	University of Cape Town
UFRJ	Universidade Federal do Rio de Janeiro

1. Introduction

Tumbling mills are cylindrical shaped equipment with the main purpose of breaking ore particle to a size where the liberation of the valuable minerals is possible. This class of equipment is among the most used in the comminution of minerals, presenting great robustness, and being capable of dealing with large tonnages of material per day and a wide size range for the feed.

Structurally, this type of mill consists of a horizontal cylindrical shell, equipped with replaceable wearing liners and a charge of grinding medium. The drum is supported so as to rotate on its axis, lifting the charge (ore particles and grinding media) and projecting it. Usually tumbling mills are of three basics types: ball, rod and autogenous. In the mineral industry, this class of comminution equipment is typically employed in coarse grinding, in which particles typically between 5 and 250 mm are reduced in size to between 40 and 300 µm (Wills & Napier-Munn 2006).

Although tumbling mills have been developed to a high degree of mechanical efficiency and reliability, they are extremely wasteful in terms of energy expended. In a typical mineral processing plant, around 35% to 50% of the operational costs are related to comminution (Curry et al. 2014). It is estimated that about 1% of the total electricity generated in the world is used in crushing and grinding operations (Norgate & Jahanshahi 2011). For ball mills, values of 15% for energy efficiency in the creation of new surface area have been estimated (Fuerstenau & Abouzeid 2002).

From the standpoint of the ore, it is estimated that the extraction of metallic minerals will continue to grow for the next decades. For metals such as copper, iron and aluminum, processing of the respective ores is expected to double by 2030. However, the ore grades should continue falling, making its processing and concentration even more difficult and expensive (Mudd 2010).

Considering all the points presented above, the modeling and complete understanding of the charge behavior and mechanisms related to particle breakage in tumbling mills are of extreme importance. Throughout the 20th century, some models relating operational conditions of mills with particle breakage have been proposed. One of the first methodologies suggested, and used until today, is the Bond Method, for the scaling of industrial mills from locked-cycle tests (King 2001). In the 1960s onwards, more complex models were proposed, considering the population balances and breakage properties of different size classes.

The approaches mentioned above, although useful, present serious limitations since they do not take into account some construction and operating characteristics of the mills, such as size and shape of grinding media, liner profile and rotational velocity of the mill shell. Those limitations come from the fact that tumbling mills are closed and opaque systems, making the complete quantification of charge distribution and motion extremely difficult or even impossible. In industrial mills, measurements of feed, discharge, power draw and mass of charge inside the mills are possible, however, information about charge motion, size distribution throughout the mill length and collision energy spectrum between ore and grinding media are still very hard to be determined. The latter is of extreme importance in the case of Greenfield projects or those that will process ore with unusual behavior.

In order to overcome this difficulty, Mishra and Rajamani applied in the 1990s the Discrete Element Method (DEM) for the first time in the simulation of mills. The discrete element method is a special class of numerical schemes for simulating the behavior of discrete, interacting bodies. Hence, by its very nature, DEM is highly suitable for the tumbling mill problem (Mishra & Rajamani 1992). It consists of applying Newton's second law to particulate bodies in motion and a force displacement model to the bodies in collision (Mishra & Rajamani 1992). In the last two decades, DEM has been widely applied in equipment and comminution process modeling, advancing with increasing computational power.

In order for a DEM simulation to describe the particle movement within a geometry with fidelity to what is observed in the real environment, it is necessary to use in the method proper material and contact parameters. Those parameters are not always known *a priori*. One way to estimate such parameters is through calibration, by quantitative comparison of experimental and simulation results. In that sense, it is advantageous to use laboratory-scale mills, where the measurement of the charge flow might be possible.

The Positron Emission Particle Tracking (PEPT) presents itself as an ideal technique for calibrating DEM parameters in some cases. PEPT is a technique for measuring the flow trajectory of a radioactive particle tracer, in three dimensions, in a granular or fluid system such as a tumbling mill, at a frequency of up to 250 Hz (Parker et al. 1993). At the end of the test, it is possible to calculate a statistical distribution of particle density in each of the tested system regions.

The main objective of the present work is to suggest a methodology for the calibration of contact parameters, for DEM simulations, using data acquired from tests in a mill using the PEPT technique. Some options of comparing PEPT and DEM are presented and the validity of the comparison itself is assessed.

2. Objective

The main objective of the present work is to suggest a methodology for the calibration of contact parameters, for DEM simulations, using data acquired from tests in a mill using the PEPT technique. Some options of comparing PEPT and DEM are presented and the validity of the comparison itself is assessed.

3. Review of the literature

3.1. Grinding

Since most of the *ore minerals*, that is, minerals that can extracted profitably, find themselves finally associated with *gangue*, which is the rocky material without economic value, its liberation is necessary. Such liberation is achieved through *comminution*, which consists in the progressive size reduction of particles down to size ranges required for subsequent concentration. Comminution represents the first stage in mineral processing after mining and in general is divided into crushing and grinding stages.

Grinding is usually the last stage in the process of comminution; in this stage particles are reduced in size by a combination of impact and abrasion, either dry or in suspension in water. It is performed in rotating cylindrical steel vessels which contain a charge of loose crushing bodies – the grinding media – which is free to move inside the mill, thus comminuting the ore particles. Figure 3.1 illustrates the main modes of application of stresses involved in grinding equipment. A special kind of grinding equipment is the tumbling mill. Tumbling mills are typically employed in coarse grinding, in which particles between 5 and 250 mm are reduced in size to between 40 and 300 µm (Wills & Napier-Munn 2006). The grinding media used in the charge generally defines the mill. Thus the medium could be steel or cast iron balls, when the mill is designated as a *ball mill*; or it could be steel rods, where the mill is known as a *rod mill*. When no grinding medium is charged it is known as an *autogenous mill.*

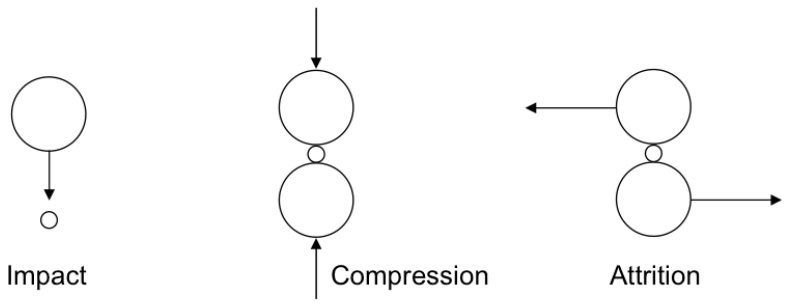

Figure 3. 1 – Types of stress mechanisms inside grinding equipment. Larger circles representing grinding media and smaller circles representing ore particles.

Grinding is usually performed wet, although in certain applications, such as cement production, dry grinding is used. When the mill rotates the mixture of grinding media, ore, and water, known as the *mill charge*, is intimately mixed, with the medium comminuting the particles by any of the three kinds of stresses cited above, depending on the rotational speed of the mill and the shell liner structure.

Several devices are used to promote size reduction of particles inside a conventional tumbling mill, such as lifters that help to raise the grinding media to greater heights before they drop and cascade down. Lifters are incorporated in the mill liners, which are designed with different profiles. They serve the dual purpose of protecting from wear the steel outer shell of the mill and help lifting the charge. Liner surfaces can be smooth, ribbed or waved. The rate of wear of liners is roughly proportional to the speed of rotation of the mill (Gupta & Yan 2006).

On rotating a mill charged with ore rocks and grinding media, the entire charge rises against the perimeter of the mill in the direction of the motion. On reaching a certain height, part of the charge cascades and falls to the bottom of the mill, while the other part tends to slip down but soon travels again in the direction of motion of the mill. Figure 3.2 illustrates the charge motion inside a mill. During these processes, the media drops repeatedly onto the rock, breaking it down to finer sizes. Some size reduction also takes place due to shear or abrasive forces. As a result of the combined action of repeated impact and abrasion over time, size reduction takes place and, given sufficient time, the mineral of interest becomes sufficiently liberated in such a form that it can be economically recovered.

Depending on the rotational speed and the degree of filling, three types of charge motion states can be distinguished: cascading, cataracting and centrifuging motion, as illustrated in Figure 3.2. At relatively low speeds, the medium tends to roll down to the toe of the mill and predominantly abrasive comminution occurs. This *cascading* leads to finer grinding. At higher speeds the medium is projected clear of the charge to describe a series of parabolas before landing on the toe of the charge. This *cataracting* leads to comminution by impact. At the *critical speed* of the mill the theoretical trajectory of the medium is such that it would fall outside the shell. In practice, *centrifugal* occurs and the medium is carried around in an essentially fixed position against the shell (Wills & Napier-Munn 2006).

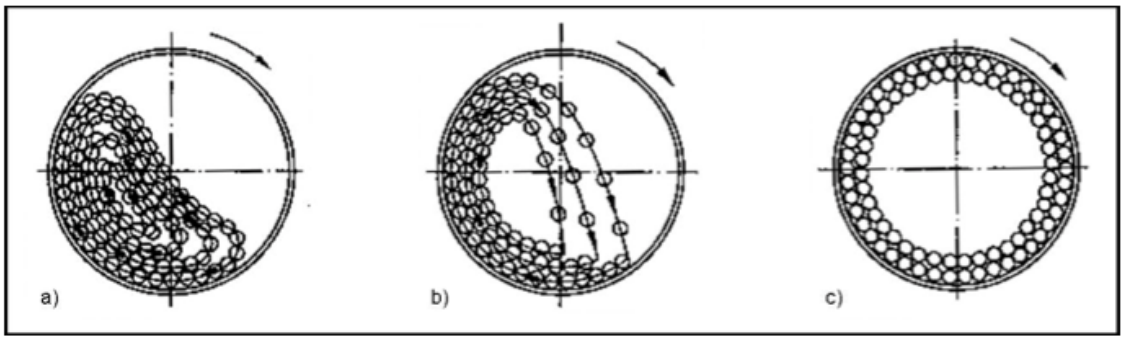

Figure 3. 2 – Charge motion inside a mill: a) cascade; b) cataract; c) centrifugal.

In order to provide a better description of charge motion in relation to mill operation and construction characteristics, some features of the charge need to be defined. Two such features are the *centre of circulation* (CoC) and the *equilibrium surface*. The CoC is defined as the point about which all the charge in the mill circulates and the equilibrium surface as the surface dividing the ascending *en masse* charge from the descending charge (Powell & McBride 2004). Figure 3.3 shows a photographic image of a batch ball mill equipped with a transparent lid and indications of some charge features. Additional charge features are the *departure shoulder* – uppermost point t which the charge departs from the shell of the mill; the *head* – the highest vertical position that the charge attains; the *bulk toe* – turning point of bulk charge against the mill shell; the *impact toe* – region, providing the mill speed is sufficiently high, where the cataracting charge impacts the shell.

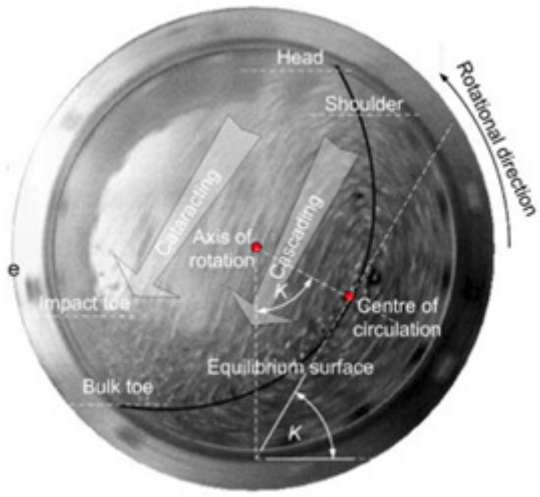

Figure 3. 3 – Charge features.

Table 3. 1 – Summary of charge definitions.

Name	Description
En masse	Bulk region of the charge moving in an upward direction
Equilibrium surface	Surface separating the rising en masse charge from the descending charge
Centre of circulation (CoC)	Axis about which all charge in the mill Circulates
Shoulder	Uppermost point at which material leaves the mill shell
Head	Highest point of the charge trajectory
Bulk toe	Point if intersection of tumbling charge motion with mill shell
Impact toe	The region where cataracting charge impacts on the mill shell

The theoretical critical speed of mill can be given, in rotations per minute, by

$$Critical\ speed = \frac{42.3}{\sqrt{D_m - d_b}} \tag{3.1}$$

where D_m is the mill internal diameter and d_b is the diameter of the grinding media, both in meters. Commonly, mill velocities are represented in terms of fraction of the critical speed.

The mill filling, also known as mill load, is the percentage of mill internal volume occupied by the grinding media and the interstices between them and can be calculated by

$$J = \frac{V_b}{V_m \cdot (1 - \varphi)} \tag{3.2}$$

where V_b and V_m are the volume of the grinding media and the internal mill volume, respectively. The charge porosity φ is the fractional volume of the interstices between the grinding media.

A key parameter defining the performance of a mill is the energy consumption. The energy supplied to the mill is primarily used to lift the charge and keep the shell rotating. The power drawn by a rotating mill has a direct correlation with the type of charge motion produced by the regime in which it operates (Wills & Napier-Munn 2006). The charge motion, and consequently, power draw has been demonstrated to be influenced by mill operating variables such as lifter height and rotational speed, as

well as charge parameters such as size and volumetric filling (Powell & Nurick 1996). Figure 3.4 illustrates how energy consumption is influenced by the mill speed. The grey area indicates the usual range applied in the industry, which is the range 65-82% of the critical speed, although values as high as 90% are sometimes used.

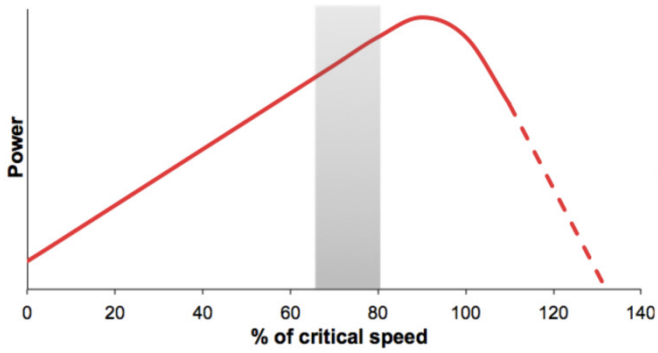

Figure 3. 4 – Influence of fraction of the critical speed on power consumption (Kelly and Spottiswood 1982).

As the mill speed increases, the centre of mass of the charge initially moves to the periphery of mill. However, as the shell approaches the critical speed, the centre of mass moves back towards the mill centre, since an increasing number of particles are held against the mill shell.

Many studies have been published that proposed equations or methodologies for predicting mill power consumption since it is of key importance in the designing stage of the equipment (King 2001). Bond proposed an empirical equation for the mill power in relation to some operational conditions, being given by

$$P = 7.33AJ\varphi(1 - 0.937J)\left(1 - \frac{0.1}{2^{9-10\varphi}}\right)\rho_b L {D_m}^{2.3}, [kW] \tag{3.3}$$

where A is a constant equal to 1 for mill with overflow discharge, 1.16 for slurry milling with grate discharge and 1.08 for dry milling (Bond 1960). L and D are the mill length and diameter, respectively, and ρ_b the density of the grinding media. As is common in empirical approaches, although simple, this equation relies on correction factors when dealing with unusual conditions. For mill with diameter smaller than 2 meters, in dry batch milling, Austin proposed an alternative empirical equation for the mill power (Austin & Concha 1994), in kW, given by

$$P = 13.0MD_m{}^{0.5}\left(\frac{(\varphi - 0.1)}{1 + exp[15.7(\varphi - 0.94)]}\right)\frac{(1 - 0.937J)}{(1 + 5.95J^5)} \tag{3.4}$$

where $M$is the mass of the ball charge, in tons. However useful in various applications, those equations do not relate the power consumption with charge variables, such as, grinding media distribution, charge elevation, porosity, etc.

Morrell (1996), on the other hand, proposed a model that uses information from mass of particles and the amount of slurry inside mills to predict charge volume, density and position. Morrell proposed an energetic approach, assuming that power is the rate at which potential and kinetic energy are transferred to the charge. Figure 3.5 presents a representative scheme of the region in the charge Morrell proposed is responsible for energy consumption. The net power, for lifting the charge, devised by Morrell is given by

$$P_{NET} = KD_m{}^{2.5}L_{EFF}\rho_b J\varphi\left[\frac{5.97\varphi - 4.43\varphi^2 - 0.985 - J}{(5.97\varphi - 4.43\varphi^2 - 0.985)^2}\right] \times \left[1 - (1 - 0.954 + 0.135J)e^{-19.12(0.954 - 0.135J - \varphi)}\right] \tag{3.5}$$

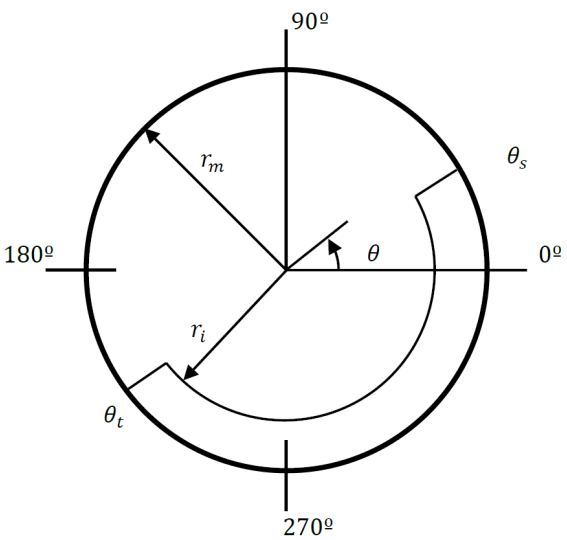

Figure 3. 5 – Mill charge scheme according to Morrell (1996).

Studies on power draw prediction based on charge motion (Hogg & Fuerstenau 1972; Liddel 1988; Morell 1993) have traditionally followed simplified descriptions of charge motion. This is mainly due to the complexity associated with accurately describing the tumbling mill environment mathematically in a fundamental level.

3.2. Discrete Element Method (DEM)

The Discrete Element Method (DEM) however emerged as a means to investigate particle motion and interaction in enclosed equipment. DEM is a numerical technique for the simulation of motion and interaction among discrete bodies. Fundamentally, DEM solves Newton's equations of motion to resolve particle motion and uses a contact law to resolve inter-particle contact forces. The contact model describes the collision mechanics between two or more particles or between particles and the geometry confining the charge. DEM was firstly developed for studies on soil mechanics, although for small number of particles (Cundall & Strack 1979). In the minerals industry, the first application was done a few years later for the simulation of grinding media motion in ball mills (Mishra & Rajamani 1992). A typical visualization of a DEM simulation is given in Figure 3.6.

For tumbling mills, DEM can be used in the prediction of charge behavior as a function of internal mill geometry, rotational speed, mill filling, etc. Some of the capabilities of DEM are (Weerasekara et al. 2013):

- Calculates the position, linear and angular velocity of all the particles in the system for each time step;
- Calculates the energy involved in collision events, for both particle-particle and particle-geometry contacts;
- With appropriate modifications, it is capable of predicting particle breakage.

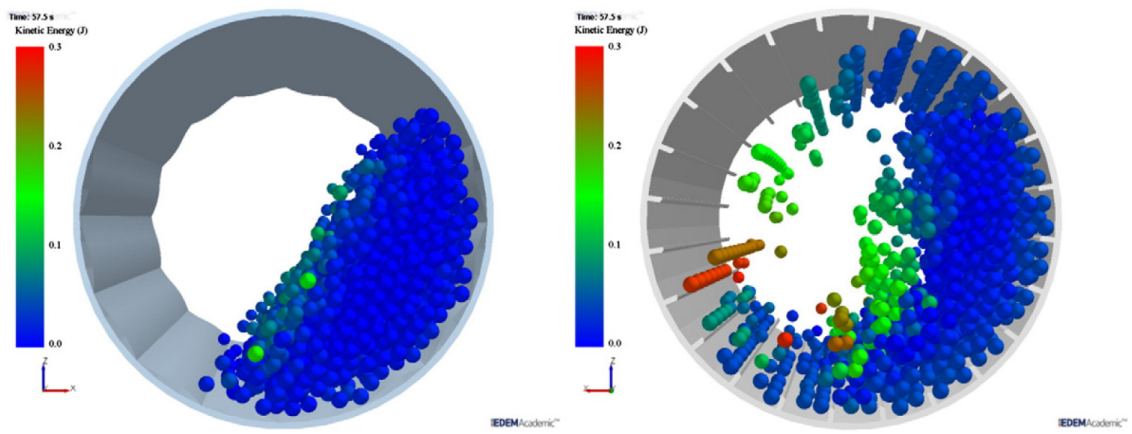

Figure 3. 6 – DEM simulation of the effect of liner design in a 0.6 m diameter mill operating at 68% of critical speed, with 30% ball filling and 25 mm steel balls (Carvalho & Tavares 2013).

In recent years, studies have been carried out on coupling DEM to others computer simulation techniques, for instance: Gustafsson et al. (2013) applied DEM-FEM coupling (finite element method) to predict bed breakage of iron ore pellet by compression; Mayank et al. (2015) used CFD (computational fluid dynamics) coupling to predict charge and slurry dynamics in tumbling mills; Cleary (2015) simulated wet grinding in a 36' SAG mill using DEM-SPH (smoothed particles hydrodynamics) coupling.

The use of coupling techniques allows the application of microscale information on a macroscale analysis of problem to be solved, providing, in principle, a more realistic simulation of the charge behavior in a equipment. However, these coupling techniques require extensive calibration of its models and along with high computational power, making its application in real size equipment still limited. Additionally validation and effectiveness of the coupling remains questionable.

Various types of contact relationships are available to describe interactions between particles. These models include contact between smooth, spherical, non-spherical, cylindrical, and non-cylindrical elastic particles with friction and surface adhesion (Mishra 2003). The Hertz-Mindlin contact model (Mindlin 1949) has been used by a number of researches to conduct DEM simulations of tumbling mills (Tavares & Carvalho 2010; Khanal & Morrison 2008; Mishra & Cheung 1999). The model is based on Hertz contact theory and utilizes the linear elasticity model of continuum environment to calculate the normal force of two perfectly elastic spheres in contact (Etsion 2010). Since in DEM particles are nondeformable, the key approach of the method is to consider the solid particles to be able to overlap and collision forces that result from the relative normal and tangential velocities.

Hertz has showed that two spherical particles of radius r_1 and r_2 in contact interact with applied normal force given by,

$$F_n = {f_n}^r + {f_n}^d = -k_r \left\| {\delta_n}^{1/2} \right\| \delta_n - \left(k_d \left\| {\delta_n}^{1/4} \right\| \right) \dot{\delta}_n \tag{3.6}$$

where δ is the deformation length of the particles. The stiffness constant k_r is given by,

$$k_r = \frac{4}{3} Y^* \sqrt{R} \tag{3.7}$$

and the restitution constant,

$$k_d = c_n\left(6m_i Y^* \sqrt{R}\right)^{1/2} \tag{3.8}$$

In these equations, c_n is the normal restitution coefficient and Y^* depends on the Young's modulus Y,

$$Y^* = \frac{Y}{2(1-\upsilon^2)} \tag{3.9}$$

on Poisson's ratio υ, and the effective radius R is,

$$\frac{1}{R} = \frac{1}{r_1} + \frac{1}{r_2} \tag{3.10}$$

The normal deformation rate, defined by $\dot{\delta}_n = (v_{ij} \cdot n_i)n_i$, is function of relative velocity v_{ij} at the contact point,

$$v_{ij} = (v_j - v_i) + [\omega_j \|r_j\| n_j - \omega_j \|r_i\| n_i] \tag{3.11}$$

where n_i is the unitary vector that its origin from particle center i respectively in direction to the contact point with the other particle involved in the contact (particle j) and vice versa. in the case of spheres submitted to an angular load, the tangential contact force is calculated by Mindlin's model (Mindlin 1949). As in the case of normal force, the tangential force applied to the particle t is the sum of the repulsion and damping terms, as

$$F_t = {f_t}^r + {f_t}^d \tag{3.12}$$

The repulsive force is calculated by,

$${f_t}^r = \mu_s \|{f_n}^r\| \left[1 - \left(1 - \frac{\|\delta_t\|}{\chi}\right)^{3/2}\right]\left(\frac{\delta_t}{\|\delta_t\|}\right) \tag{3.13}$$

where μ_s is coefficient of static friction and,

$$\chi = \mu_s \frac{2-\upsilon}{(2-2\upsilon)\|\delta_n\|} \tag{3.14}$$

is the maximum tangential deformation before slip occurs. In order to satisfy Coulumb friction law, this force is limited to $\mu_s {f_n}^r$, which results in the relation, $0 \leq \|\delta_t\| \leq \chi$.

The restitution force is proportional to the tangential deformation rate at the contact point, $\dot{\delta}_t$,

$$f_t^d = -c_t \left(6 m_i \mu_s \| f_n^r \| \frac{\sqrt{1 - \frac{\|\delta_t\|}{\chi}}}{\chi} \right)^{1/2} \dot{\delta}_t \tag{3.15}$$

where c_t is the tangential restitution coefficient and the tangential deformation rate is,

$$\dot{\delta}_t = v_{ij} - (v_{ij} \cdot n_i) n_i \tag{2.16}$$

The acting torque on particle i when it collides against a particle j, may be modeled by the product of the force acting on the particle and its radius. The resulting torque can defined as the rolling friction torque, given by,

$$T_i = -\mu_r \| f_n^r \| \frac{\omega_i}{\|\omega_i\|} \tag{3.17}$$

where μ_r is the rolling friction coefficient.

All forces on each of the objects and particles are, then, summed and the following equations of motion are integrated:

$$m_i \frac{dv_i}{dt} = \sum (F_{n_i} + F_{t_i}) + g \tag{3.18}$$

$$I_i \frac{d\omega_i}{dt} = \sum T_i \tag{3.19}$$

In these equations m_i and I_i refers to the mass and moment of inertia of particle i and v_i and ω_i are their linear and angular velocities.

The key parameters in this model are the coefficient of restitution and the coefficient of friction. The coefficient of restitution can be defined as the ratio v/v_0, where v and v_0 are, respectively, the particle velocity before and after a collision event (Johnson 1985).

The coefficient of friction is difficult to measure, and it may vary during grinding (Mishra 2003). While Cleary (1998) seemed to suggest that power draw is relatively insensitive to the choice of value for coefficient of friction, Mishra & Rajamani (1992) and van Nierop et al. (2001) showed that power draw of ball mills indeed depends on the

coefficient of friction, and it is particularly sensitive at higher mill speeds, as is shown in Figure 3.7.

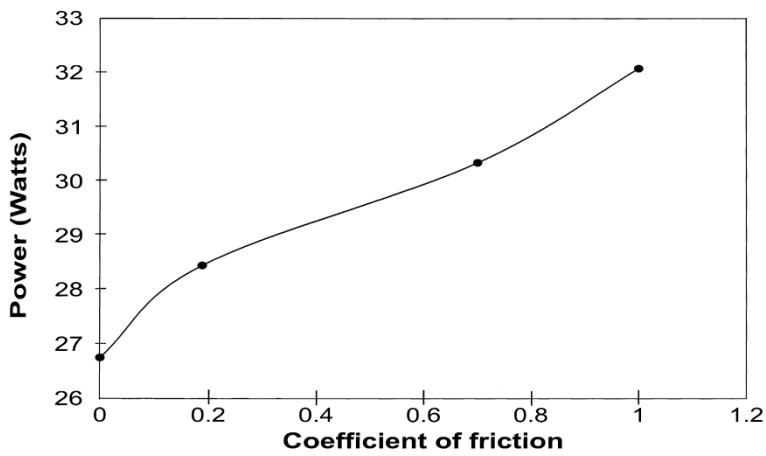

Figure 3. 7 – Effect of the coefficient of friction on mill power draw (van Nierop et al. 2001).

These parameters however are not intrinsic material property, depending on the materials of the bodies in contact, their surface geometry and the impact velocity (Johnson 1985), making the measurement or experimental determination of their values a difficult task.

As numerical modeling of tumbling mills using DEM has gained acceptance, many researchers directed their work into validating DEM simulations. Calibration of the parameters used for the contact model normally involves experimental measurement of a simplified system, while validation of the simulations results entails mainly three approaches:

- High speed filming/photography
- Sensor measurements
- X-ray and PEPT imaging

In some studies, such as in those by Venugopal & Rajamani (2001); Dong & Moys (2003); Pérez-Alonso & Delgadillo (2012); van Nierop et al. (2001), a laboratory scale mill with a transparent end face and a mounted camera has been used, as shown in Figure 3.8. The high speed camera captures snapshots or videos of the moving charge, under different conditions, and the images are then compared to DEM simulations at identical conditions. The accuracy of the simulations is then verified by

comparing the charge shape and distinguishing features such as toe and shoulder in experiments and simulations.

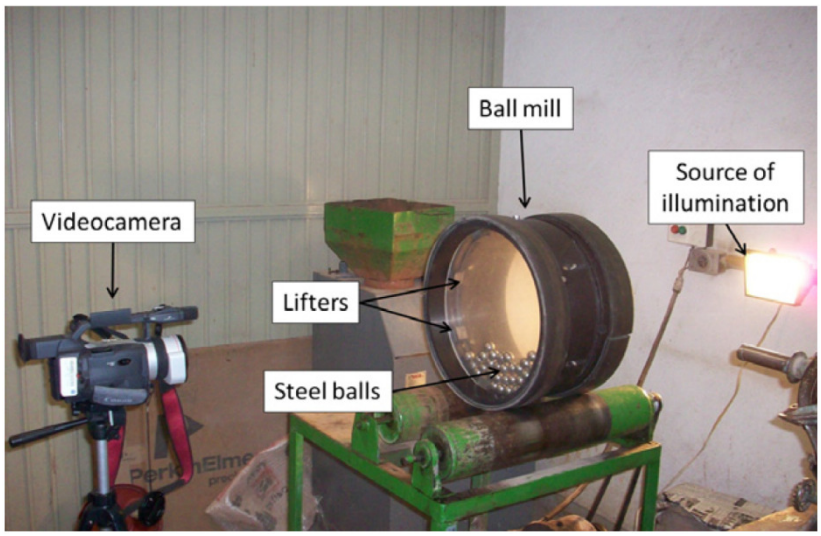

Figure 3. 8 – Experimental setup used for validation of DEM simulation by Pérez-Alonso and Delgadillo (Pérez-Alonso & Delgadillo 2012).

The main advantage of this system is that it is actual charge motion that is compared to those obtained from DEM simulations. Influence of operational conditions on charge motion can be related to experiments and simulations. However, the drawback of this approach is that it is a qualitative observation of the accuracy of DEM, being highly subjective as the images can be selected as to match the simulation. While this method is a good measure of observable features, such as the head and toe positions, it does not provide the means for a quantitative evaluation of inter-particles forces or the energy environment in the mill.

Another form of calibration is through online sensor measurements usually by instrumentation of the mill. The power raw of tumbling mills is typically measured via torque sensors attached to the system. Additional sensing is sometimes applied in order to quantitatively measure charge features. In a study carried out by Kiangi et al. (2013) an inductive proximity probe and steel ball as charge were used, as shown in Figure 3.9. The probe detects the presence of metallic objects in the proximity of its sensing face. This technique has the advantages of being able to detect the position of the steel media load and give accurate measurement of the toe and shoulder's angular positions. Although these approaches provide more precise information on charge

features, as in the case of the technique discussed previously, it does not resolve the particle motion in the bulk of the charge.

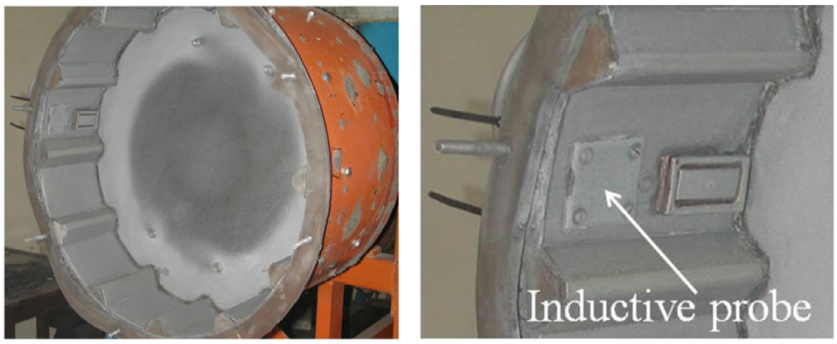

(a) Photograph of the mill (b) Inductive probe installation

Figure 3. 9 – Tumbling mills fitted with inductive proximity probe (Kiangi et al. 2013).

Another approach is imaging of the internal mill environment through X-ray measurement or particle tracking via gamma ray emission (PEPT), the latter will be better explained in the following session (Govender et al. 2001; Yang et al. 2003). In those methods, the motion of particles inside the tumbling mill is traced and used to ascertain information on the overall charge behavior. Although it does not provide details regarding inter-particles forces, kinematic information is obtained for particles subject to those forces. A photograph of such system is presented in Figure 3.10.

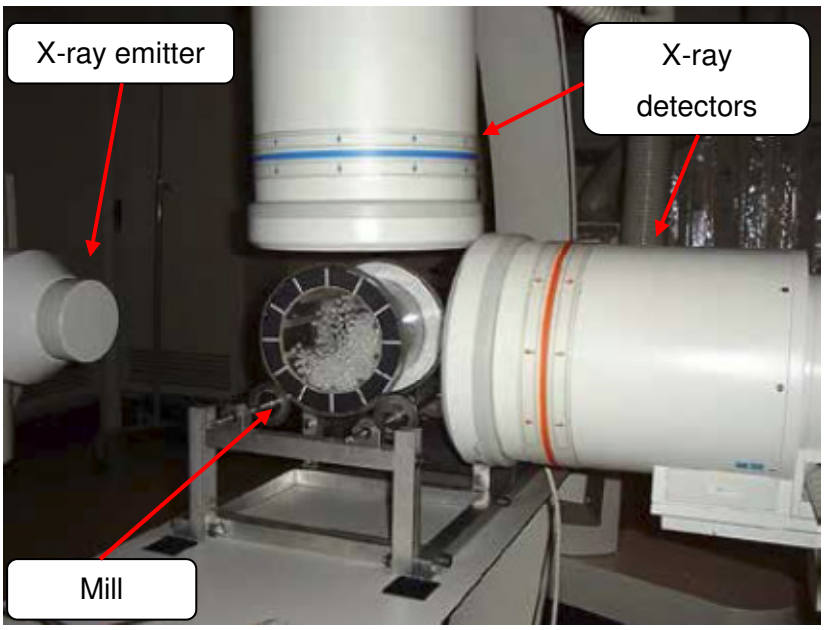

Figure 3. 10 – Photograph of biplanar X-ray imaging system (Govender et al. 2001).

The advantage of this method is that it is a quantitative measure of charge motion in the environment which is being validated. Some kinematic properties such as velocity distribution can be directly compared against DEM data. One disadvantage of using this type of technique is that it requires the use of an equipment with materials that permits radiation passage. An additional limitation is that the equipment has to fit inside the field of view of the camera system, that is, the size of mill that can be tested is limited by the instrumentation available.

The PEPT technique then offers a unique opportunity for validation of DEM simulations since it resolves particle motion in the bulk of the charge. PEPT, which is utilized in this study, is discussed in more detail in the next section.

3.3. Positron Emission Particle Tracking (PEPT)

Positron emission particle tracking (PEPT) has been developed at the University of Birmingham, U.K., and presents great potential for elucidating mechanisms in a variety of processing units. PEPT is a technique for following the motion of a radioactively labeled tracer particle. Like the more established imaging technique of positron emission tomography (PET) it uses a radionuclide which decays by positron emission, and relies on detecting the pairs o back-to-back γ-rays produced when positron annihilate with electrons. These γ-rays are very penetrating and an accurate location can be determined from detection of a small number of back-to-back pairs, so that non-invasive tracking is possible inside actual engineering structures. The technique is only restricted by the availability of suitable positron cameras (Parker et al. 1997).

The tracer is then placed in the system within the field of view of a positron camera. The gamma rays are detected by positron detectors and the very high number of photons emitted allows the tracer position to be found by triangulation. The process can be repeated a few thousand times per second making it possible to track the tracer. Figure 3.11 shows a picture of the PEPT system from iThemba LABS (University of Cape Town), along with a schematic of the triangulation. Knowing the tracer position over time allows the visualization of charge motion and hence information such as the velocity, the occupancy, dispersion, etc, to be calculated (Parker et al. 1994).

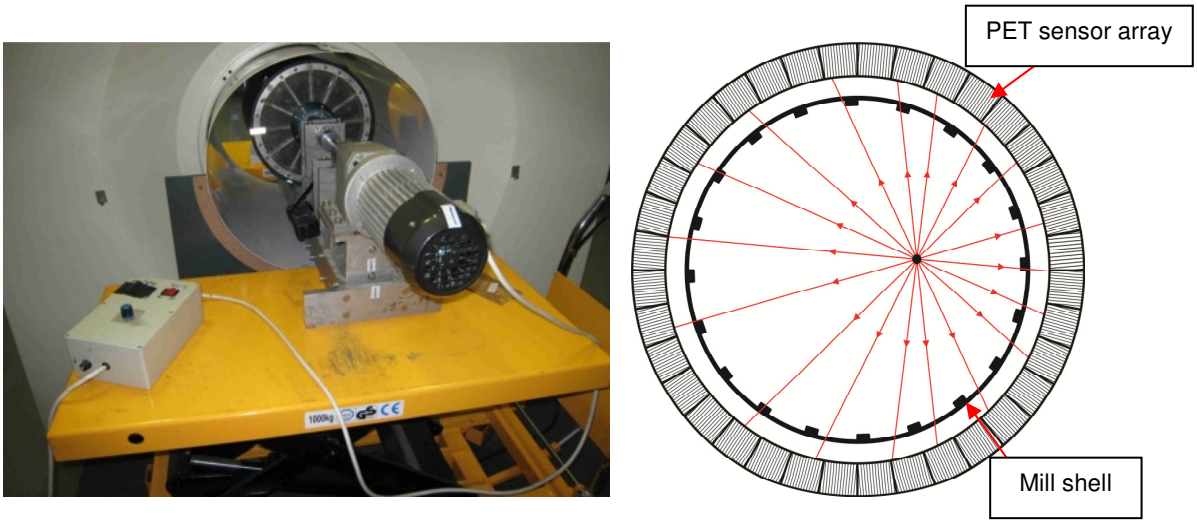

Figure 3. 11 – Laboratory scale tumbling mill in PET camera and schematic of the triangulation.

The main assumption behind the use of PEPT in determining characteristics of the whole charge is that the system is ergodic. Ergodicity refers to the assumption that the time average of a single realization of a system can be used to determine the ensemble average (Oliveira & Werlang 2007). The hypothesis was first proposed by Boltzmann, stating that "for large systems of interacting particles in equilibrium, the time average along a single trajectory equals the space average." For PEPT, the ergodic hypothesis can be used to relate statistical data from a single tracked particle to the behavior of the whole charge in a mono-sized system, i.e., the amount time a tracer particle spends in a given segment of the system is proportional to the particle number of that segment.

Ergodicity has been demonstrated in rotating drums by Baumann et al. (1994). However it should be noted that ergodicity may not always hold. In particular, this would happen when the system is operated under centrifugal regime. In this case, particles may be stuck in separate trajectories. Thus a single tracer would not represent the whole system (Sichalwe et al. 2011). Another critical scenario is in the presence of dead or stagnant regions of flow.

The work done by Sichalwe et al. (2011) demonstrated that PEPT could be used to obtain spatial distribution of charge porosity in a rotating drum, using a single particle tracer, by initially determining the residence time fraction (RTF) spent by the tracer in each mill region. The RTF gives the probability of finding the tracer in a particular mill region and can be related to the charge particle density in this region. The spatial distribution, as shown in Figure 3.12, indicates the influence of mill speed in charge porosity, with the porosity being the inverse of the RTF.

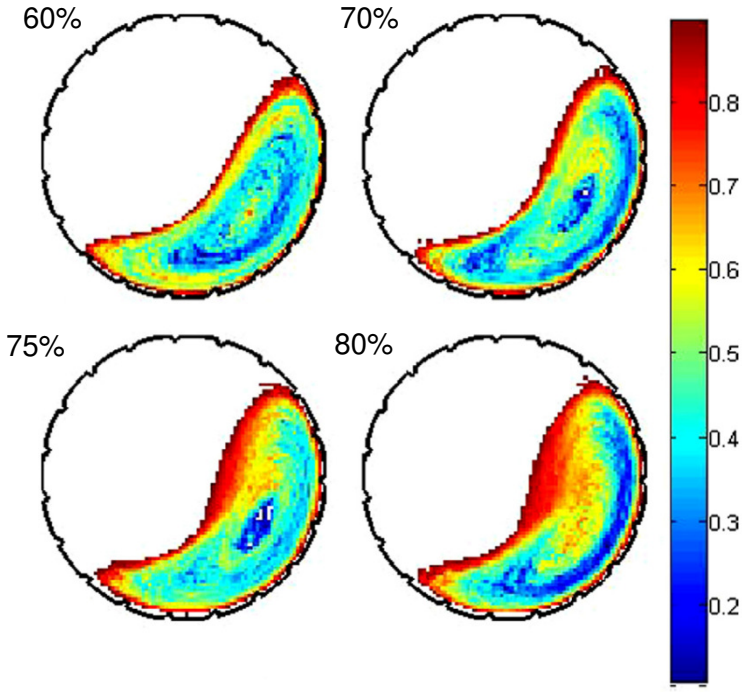

Figure 3.12 – Spatial distribution of porosity at different mill speeds, with a Rosin-Rammler distribution of glass beads at discrete sizes of 2-8 mm in a 300 mm diameter mill (Sichalwe et al. 2011).

PEPT can also be used to investigate charge power draw in tumbling mills. For instance, similarly to Morrell, Bbosa et al. (2011) proposed an energetic approach for the power draw based on the hypothesis that the mill energy is expended on lifting and rotating the charge. Bbosa states that a more accurate estimate of the power draw would be to sum up the individual "torque arm" power contributions of every internal region of the mill. The power calculation is done by dividing the mill internal volume into discrete voxels and the charge properties inside the voxel region are averaged in time. Figure 3.13 presents a diagram illustrating the calculation and the power draw, which is given by

$$P = \frac{M \cdot g}{T} \sum_{i=1}^{n} x_i \cdot l_i \cdot \bar{\alpha}_i \tag{3.20}$$

where l_i gives the fraction of the charge inside the voxel i, M the total mass of the charge, g the acceleration due to gravity, T the total time of the experiment and n the total number of voxels. x_i denoted the horizontal coordinate of the cell, while $\bar{\omega}_i$

denoted the average velocity of the voxel - calculated using the average tangential velocity divided by the radial position of the voxel.

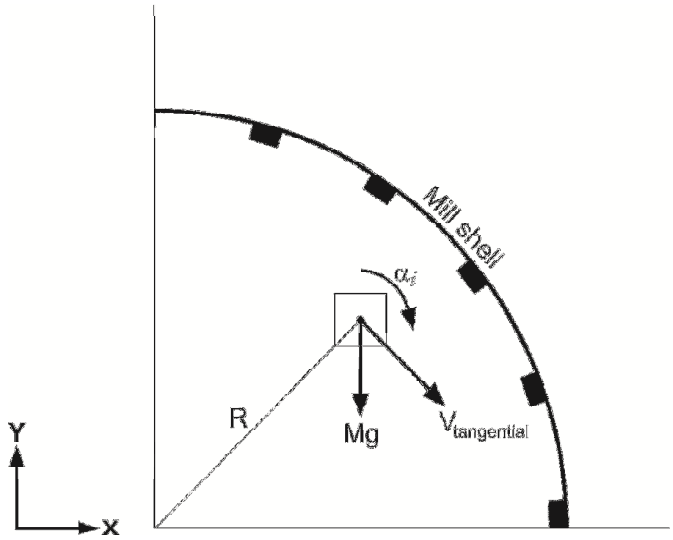

Figure 3.13 – Diagram illustrating power draw calculation.

From discrete region method utilized by Bbosa, spatial distributions such as Figure 3.14 could be plotted to examine significant areas that contributed to the charge power draw. Similarly to Morrel's model, the plot indicated that the highest contribution to the mill power draw was the bulk of the charge. In a later work Bbosa et al. (2012) compared the same data with DEM simulations having found power draw values, for both PEPT and DEM within statistical agreement.

Since no appropriate characterization processes exists for measuring friction coefficient in the presence of interstitial water, Govender et al. (2013) applied PEPT data, from wet milling, to calibration of DEM contact friction coefficient. The DEM simulations were conducted without a wet environment and the friction coefficient was adjusted in order to compensate the absence of fluid. The overall particle flow structure in a friction-adjusted DEM model was found to present small differences, as shown in Figure 3.15, to that of time-averaged velocity and porosity distributions derived from PEPT experiments considering the absence of the fluid contributions in the simulations.

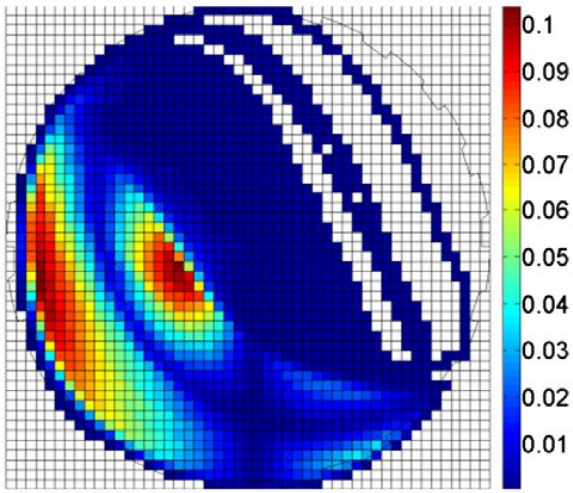

Figure 3. 14 – Spatial plot of the power draw distribution in Watts at 60% of critical speed, for 31.3% mill filling of monosize 3 mm glass beads in a 300 mm diameter mill (Bbosa et al. 2011).

In comparing DEM and PEPT data it is important to be aware that PEPT uses time averaging of one hopefully representative particle while DEM uses spatial averaging of all the particles. Depending on the nature of the device being investigated and the nature of the particles and their properties distributions, these different averages may or may not be equivalent and this can potentially add significantly to the complexity of making valid comparisons. This is further complicated if the tracer is not of the same material as the rest of the bulk material as this introduces the possibility of size, density, shape and frictional segregation. This may cause the tracer to preferentially occupy some regions of the device in an unequal way resulting in non-representative weightings in the PEPT averages over the phase space.

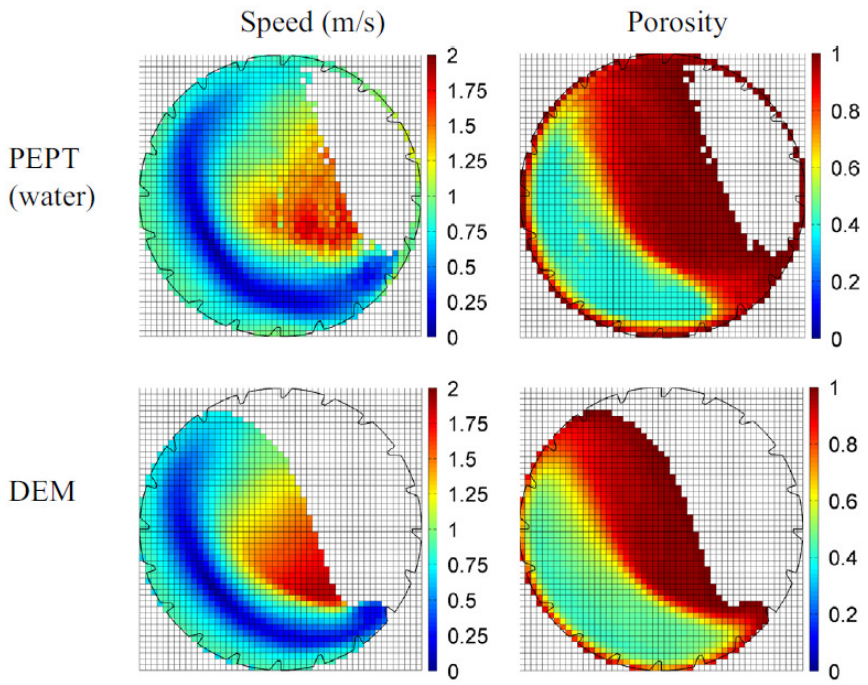

Figure 3.15 – Absolute velocity and porosity plots for PEPT and DEM at 75% of critical speed, for 31.3% mill filling of monosize 5 mm glass beads in a 300 mm diameter mill (Govender et al. 2013).

4. Materials and methods

4.1. PEPT charge motion experiments

For this study three dry tests with only grinding media as charge were performed, varying mill speed. Single particle tracking experiments using PEPT were conducted using the ADAC Forte parallel plate camera at the Positron Imaging Centre, installed at the University of Birmingham, consisting of two heads, each containing a single crystal of NaI(Tl) scintillator, 500 x 400 mm^2, optically coupled to an array of 55 photomultiplier tubes (Parker et al. 2002). Tracking was possible over the volume between the two front faces of the detectors, giving a maximum field of view of 800 x 500 x 400 mm^3.

A laboratory scale tumbling mill, with an internal diameter of 300 mm and 270 mm length, was used in the tests. Figure 4.1 shows a picture of the mill used and a schematic of its internal geometry. The mill shell was composed of high density polyethylene (HDPE) and fitted with 20, evenly spaced, nylon lifters with a height of 5 mm, width of 20 mm and 60 degree face angle. Both end faces were also composed of HDPE, possessing one an inlet and the other a discharge panel with holes of 1 mm diameter. A T20WN torque transducer (HBM 2012) was mounted between the mill and the drive motor, and used to measure torque applied and power to the mill shaft during rotation.

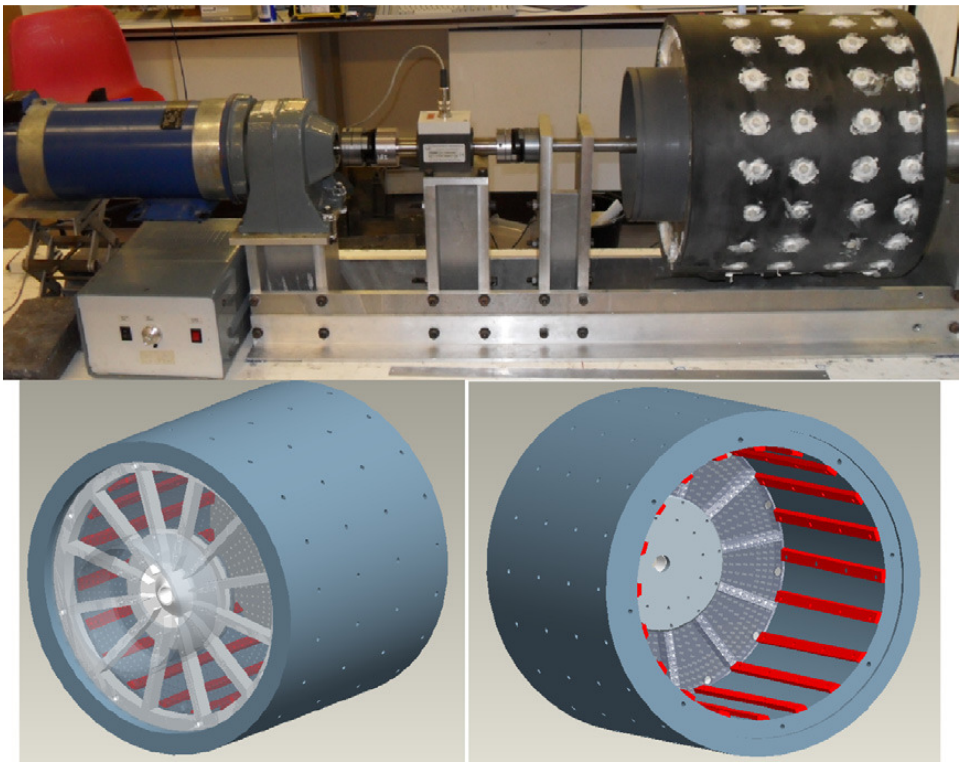

Figure 4. 1 – Tumbling mill settings and internal schematic.

Five-millimeter spherical glass beads were used as charge, comprising a constant volumetric mill filling of 31.3%. The total mass of the charge inside the mill was calculated using the equation 4.1,

$$M = (1 - \varphi) \cdot J \cdot V_M \cdot \rho_B \tag{4.1}$$

being V_M the mill internal volume, J the mill filling, and ρ_B and φ are the charge density and porosity respectively. The glass bead density was 2500 kg/m³. The porosity represents the fraction of the volume occupied by the charge, in the mill, which is empty space. There are various protocols to determine the random close packing of spheres with the same diameter, and the resultant porosity is dependent on the protocol employed (Torquato et al. 2000). The densest possible in a three dimension packing is the close-packed hexagonal structure, which has $\phi \approx 0.26$. However, in a vibrating or dynamic system, such an orderly configuration is not realistic and values around $\phi = 0.40$ are usually assumed (Jaeger & Nagel 1992). In a work done by Bbosa (Bbosa et al. 2011) using the same batch of PEPT data, a porosity of 0.37 was assumed with good agreement with the experimental results, thus the same value was used in the present work.

A single 5 mm glass bead was subjected to direct activation using a 33MeV ^{3}He beam for use as radioactive tracer particle. Following the methodology described by Parker et al. (1997), the bead was labeled with ^{18}F, which has a half-life of approximately 110 min. Before and after each test, the radioactivity of the tracer particle was measured using a Geiger counter. This was done to ensure that the level of radioactivity on the tracer was at least 300 μCi, which was the recommended minimum for the parallel plate PEPT camera (Parker & Fan 2008). In each test, the activated glass bead was added to the charge in the mill and its motion was tracked for an hour.

All the experimental procedures done for this work were performed by Centre for Mineral Research at the University of Cape Town (CMR-UCT) and shared with the Laboratório de Tecnologia Mineral - COPPE/UFRJ.

4.2. Processing of the PEPT data

The output of the triangulation algorithm, used to extract the PEPT data, was a text file which contained the Cartesian coordinates of the tracer for the duration of the experiment, after steady state has been reached. The 3D data points, in millimeters, and with time *t* in milliseconds were then imported into a MATLAB® routine for the PEPT data analysis.

For convenience, the origin is specified as the mill center, with coordinates *x* (horizontal) and *y* (vertical) in the transverse plane, while *z* along the axial mill length with zero at the one of the end faces. The triangulated coordinates, positions *x, y* and *z*, could be parameterized with respect to time *t*, as shown by the points in Figure 4.2. From the parameterized coordinate a cubic spline interpolation was done, with even time intervals, thus a more detailed trajectory could be approximated (line in Figure 4.2).

Figure 4.3 shows a plot of tracer position along the mill length against time for the test conducted at 60 mill critical speed. As can be seen from the figure the tracer position is evenly distributed along the length of the mill, not showing a tendency to occupy any particular region. In fact, for the test presented in the figure, the average mill length position kept by the tracer is 139.7 mm, roughly positioned in the middle of the mill. Thus, as the mill was run in batch mode, it was assumed that tracer's position was axially symmetric. Considering this assumption, for further analysis, the milling operation was treated as two-dimensional. Additionally, data 50 mm from the end faces

were removed from the calculations in order to avoid any border effect. Thus, the length used for the analysis was 170 mm. Figure 4.4a presents a superposition of the tracer's coordinates in the transverse mill plane at 60% critical speed and, at Figure 4.4b, its interpolated trajectory.

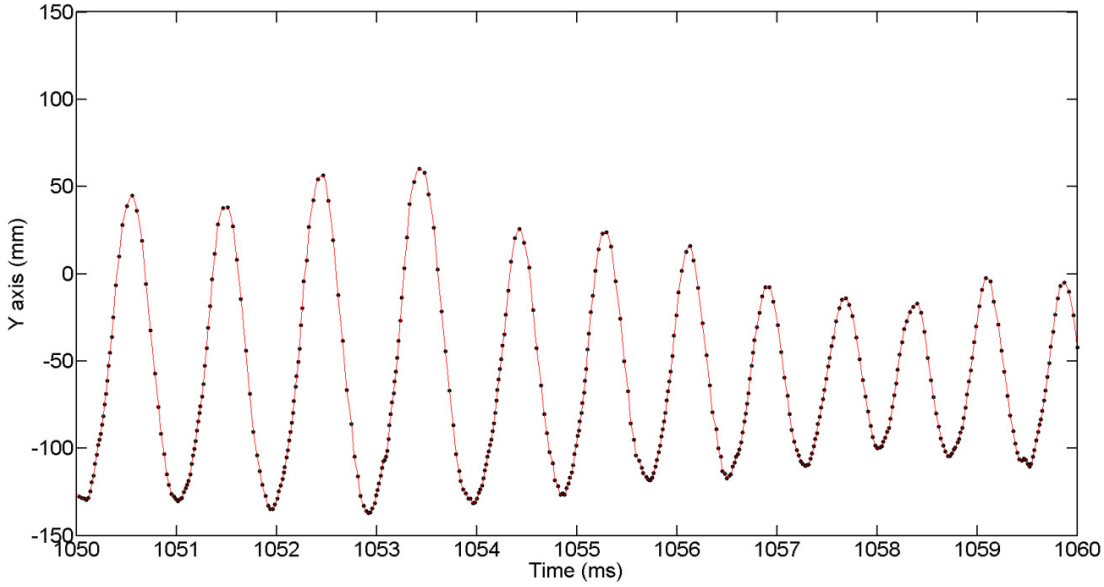

Figure 4.2 – Tracer's vertical coordinate parameterized with respect to time (points) and interpolated trajectory (line).

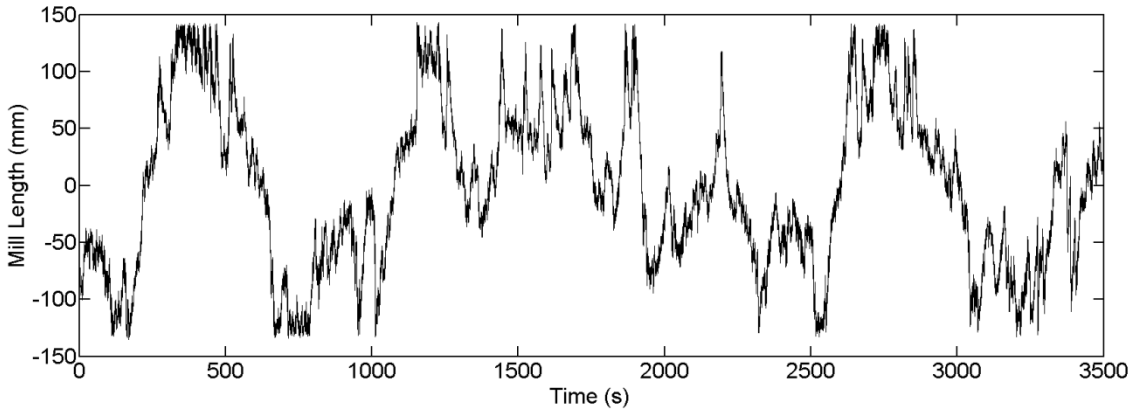

Figure 4.3 – Tracer's position along the mill length over time.

According with the ergodic hypothesis, discussed previously, the average motion properties for the tracer, over long periods of time, were considered representative of the monosize charge behavior.

In order to attain a time averaged spatial distribution of the tracer's motion in different regions of the mill, its azimuthal plane was discretized in a square grid of 50 x 50 cells. For the 300 mm mill, each cell is 6 mm in length. From the interpolated trajectory it was determined the time spent by the tracer in each region of the mill and the location

probability, i.e. as the probability of finding the tracer in a particular region of the mill. As the PEPT experiments were conducted under steady state conditions, due to the ergodic hypothesis, the location probability distributions of the single tracer particle could be interpreted as probability distributions for the entire monosize charge body. Additionally location probability gives the charge particle density throughout the mill. Spatial distribution of location probability can be determined by accumulating and normalizing the frequencies with which the tracer coordinates fell within each cell in the grid. More details of this methodology can be found in Sichalwe et al. (2011).

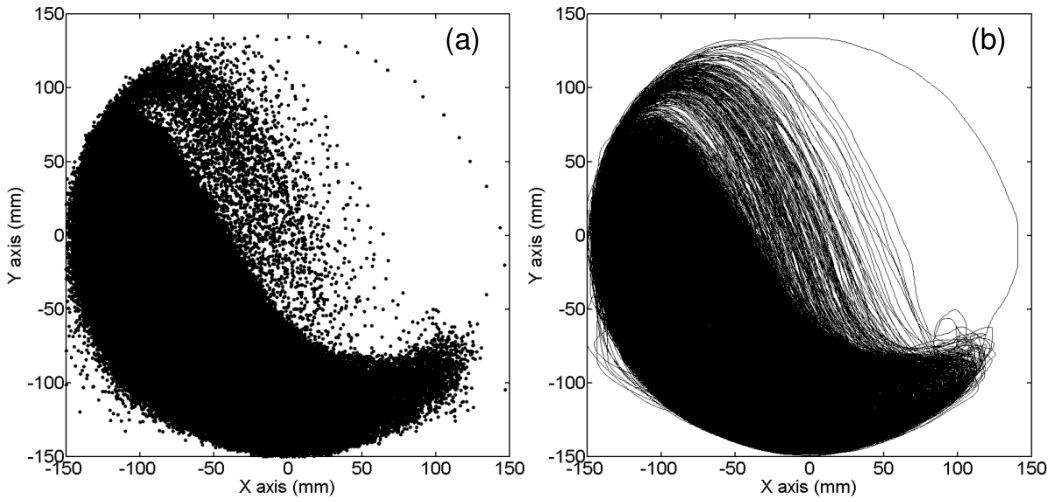

Figure 4. 4 – PEPT tracer's coordinates (a) and interpolated trajectory (b) at 60% of the critical speed.

A simple quantitative way to compare PEPT data from different experiments is the particle distribution along the two axes, horizontal and vertical, on the transversal plane of the mill, indicating the proportion of particles along the axes in relation to the total number of particles. Figure 4.5 presents an example of such distributions.

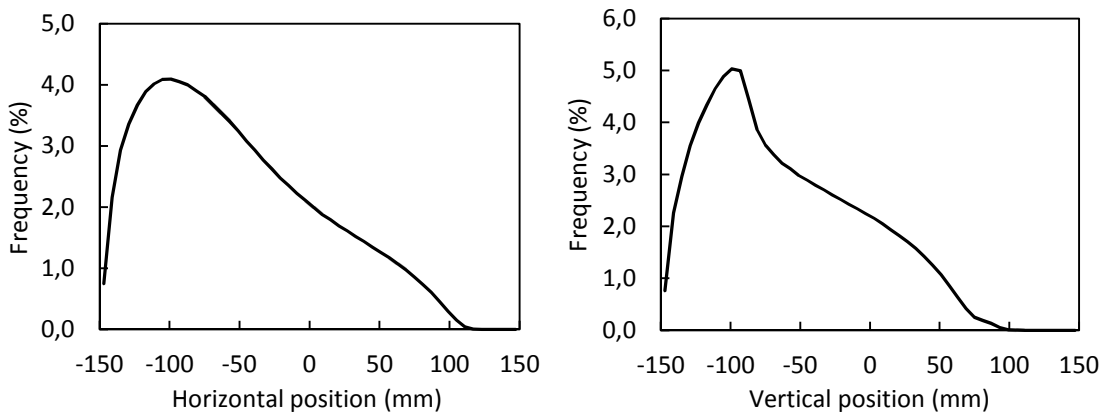

Figure 4. 5 – PEPT tracer's coordinates (a) and interpolated at 60% of the critical speed.

Having the positions of the tracer over time, it was possible to calculate its velocity and, then, a distribution of the average absolute velocities at each grid location for the charge body. Considering the particle velocity, an additional simple way of comparing PEPT data is by the distribution of velocities, which gives the proportion of time that the particle spends in particular absolute velocity. Figure 4.6 shows an example of the distribution of velocity at 60% critical speed. The distribution of velocities is usually normalized by mill rotational speed in order to allow comparison at different fractions of mill speed.

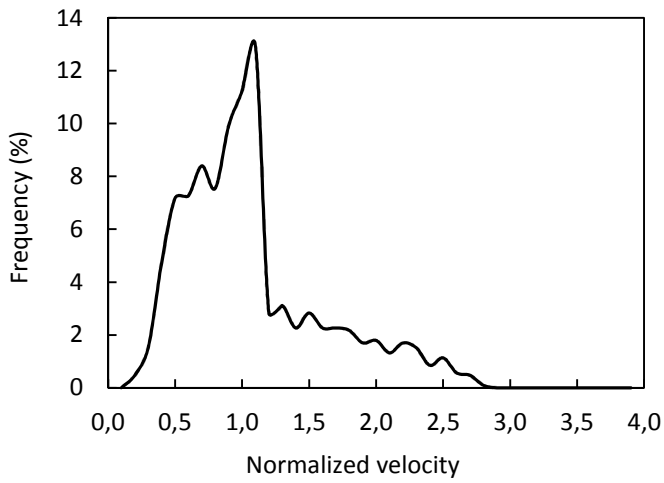

Figure 4. 6 – PEPT tracer's coordinates (a) and interpolated at 60% of the critical speed.

The power draw by the mill to lift the charge was calculated following a methodology developed by Bbosa et al. (2011) based on the hypothesis that a more accurate estimate of the power draw would be to sum up the individual "torque arm" power contributions of every cell. The mass of each cell was computed by multiplying the location probability by the total charge mass, where x_i denoted the horizontal coordinate of the cell, while $\overline{\omega}_i$ denoted the average velocity of the cell - calculated using the average tangential velocity divided by the radial position of the cell, as shown in Figure 4.7. By this method, the power draw was determined using the method developed by Bbosa et al. (2011), equation 3.20.

4.3. DEM simulations

To run the DEM simulation the commercial software EDEM®, version 2.7, was used, provided by DEM Solutions Ltd (UK). The software chosen allows quick construction of the simulations and provides good visual representation of the charge motion. Its quantitative analysis, however, is a challenging task and is described below.

For the case of the tumbling tests done with PEPT, in which the particles are only glass balls, the Hertz-Mindlin no-slip contact model (Mindlin 1949) is applicable. The material intrinsic parameters, such as density, shear modulus and Poisson's ratio, required by the contact model, were provided by manufacturer and are presented in Table 3-1.

Table 4. 1 – Material parameters for DEM simulations.

Material	HPDE	Nylon	Glass
Density (kg/m³)	950	1100	2500
Shear modulus (GPa)	0.31	0.76	26
Poisson's ratio	0.42	0.76	0.23

The mill geometry was drawn in computer aided design (CAD) software, including lifter and end faces, and imported into EDEM®. By default, in EDEM® particles are of spherical shape, and as such the mill charge could be created directly, associating its material as glass. The number of particles for a simulation of the entire mill, considering a 31.3% mill filling, was calculated using equation (3.1) as about 58,000. Figure 4.8 shows a snapshot of a simulation in EDEM®. In the figure one of the end faces has been removed for viewing purposes.

The extraction of the DEM data was carried only for the last 1.5 seconds of simulated time, after steady state has been reached, which gives a total of 4 seconds of simulated time. 1.5 seconds represents a little more than 1 revolution for 75% mill critical speed. In a preliminary simulation, with the full mill geometry and 58,000 particles, at 60% mill critical speed, in a computer with a 4 cores processor of 3.20 GHz and 8.0 Gb of RAM, the elapsed computation time was 41.3 hours for 4 seconds of simulated time. That amount of time is unpractical for the number of simulations usually done for calibration. In that sense, and considering the assumed even distribution of the charge, throughout the mill length, only a 20 mm length slice, in the middle of the

mill, was simulated using periodical domain. In that way the elapsed computation time was reduced to about 4 hours per simulation.

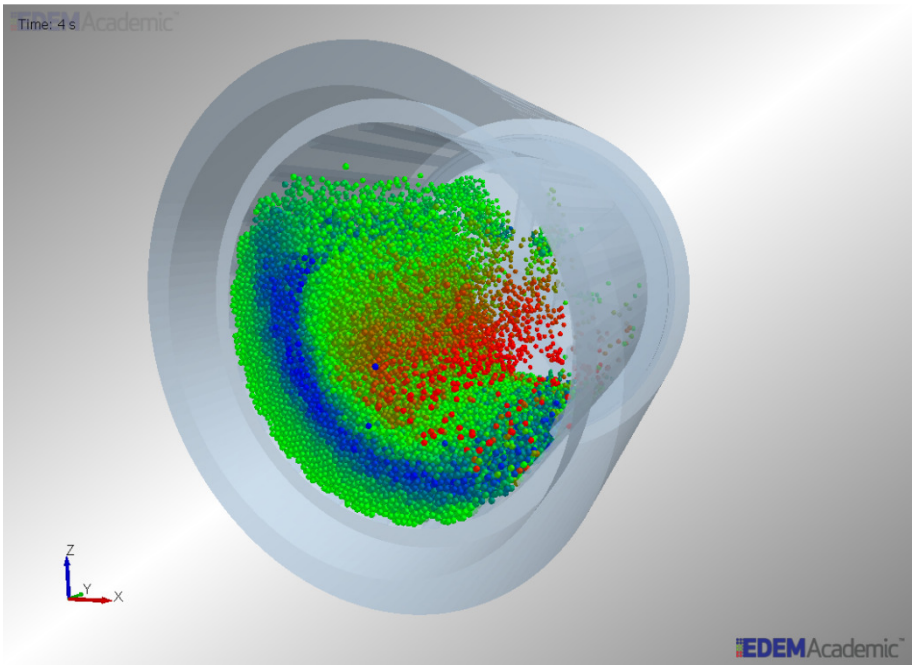

Figure 4. 7 – Snapshot of a DEM simulation at 60% critical mill speed.

Unlike in the PEPT experiment, DEM simulations record the position and velocity of each particle for a selected time step. In that sense DEM extracted data could be treated similarly as PEPT data, however, without the need for trajectory interpolation. The spatial information as particle density, spatial velocity distribution, and power distribution, could be determined for each mill region for every time step of the simulation. Once the data have been extracted at steady state of milling, the information concerning each cell could be averaged out over time.

The error for the power draw, unlike the case for PEPT data, was the standard deviation of the calculated power over time. In Figure 4.9 an example of power draw variation over time is presented.

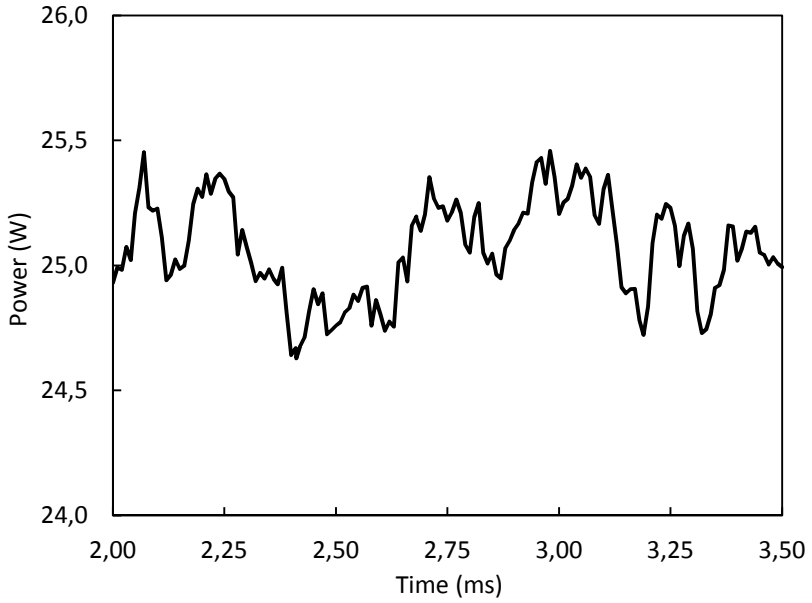

Figure 4. 8 – Power draw predicted over time for DEM simulation at 60% c.s.

4.4. Calibration methodology

The calibration of the DEM contact parameters was done using only the PEPT data experiment at 75% c.s. Thus the competence of the methodology in finding suitable contact parameters using only one experiment could be tested against two other different conditions.

The contact parameters calibrated were the coefficient of restitution and the coefficient of static friction. In order to simplify the calibration and reduce the number of simulations required it was assumed that the contact parameters for the ball-HPDE (mill shell) and for the ball-nylon (lifters) were the same. This simplification has been applied in previous studies with similar experiments, in which the DEM simulation results were satisfactory (Bbosa et al. 2012; Govender et al. 2013; Yang et al. 2003). As such, the four calibrated contact parameters were as is presented in Table 3-2.

Calibration has been carried out in stages, adding more levels of complexity at each stage. The first stage was a preliminary design of simulation experiments conducted with the purpose of verifying the influence of the four contact parameters on the correspondence between simulations and PEPT experiments. The first design of simulation experiments was a fractional factorial plan, varying the four contact parameters in two levels.

Table 4. 2 – Summary of calibrated contact parameters

Coefficient	Particle contact	Acronym
Restitution	Particle	CRPP
	Geometry	CRPG
Friction	Particle	CFPP
	Geometry	CFPG

With the aim of avoiding a biased result, the choice of the two levels, for the first design, was not based on any previous study. Considering that by definition the coefficients may vary in a range of 0 to 1, the minimum and maximum levels were arbitrarily chosen as 0.3 and 0.7. Additionally three central points were added to the design, with values of 0.5 for the four parameters included to evaluate the linearity assumption on the effects in the analysis of variance of the design.

A second more complex design of simulation experiments followed the conclusions of the first, considering only the parameters that were found to be significant to the results. The second design was a central composite design (Montgomery 2013) structured in order to estimate the optimal set of contact parameters. More details on the simulation experiments will be discussed in the following section.

In order to analyze the effect of the tested parameters an objective function was proposed. This objective function considers three forms of comparisons between DEM simulations and PEPT experimental data: two related to the charge movement inside the mill (particle and velocity distribution) and the power draw, which is easily and typically measured in industrial and laboratory scale mills. It is given by

$$Obj.func. = |P_{PEPT} - P_{DEM}| + RMS(|PD_{PEPT} - PD_{DEM}|) + RMS(|VD_{PEPT} - VD_{DEM}|) \quad (4.3)$$

where P is the power draw, PD and VD stand for the particle and velocity distribution, respectively. The term $RMS(|PD_{PEPT} - PD_{DEM}|)$ is the root mean square of the difference between particle distribution for PEPT and DEM data, whereas the term $RMS(|VD_{PEPT} - VD_{DEM}|)$ is the root mean square for the velocity distribution difference. This objective function quantifies the divergence between the PEPT and DEM charge movement. In this sense, the optimal contact parameters set should minimize this function.

5. Results and discussion

5.1. PEPT experiments results

In this section the results and analysis of the PEPT experiments run at dry batch milling, for a monosize charge of 5 mm spherical glass beads, at 50, 60 and 75% critical speed, are presented.

In Figure 5.1 the coordinates of the tracer are superimposed, indicating the charge movement profile for the PEPT tests. In these images, the mill was rotating clockwise. At 50% critical speed, the charge movement is mainly of the cascading type, with small portion of the particles being projected. However, as the mill speed increases the fraction of cataracting increases, moving the impact toe, region where the projected charge impacts with the free surface, in the direction of the charge toe, which is the region where the cascading charge encounters the mill shell.

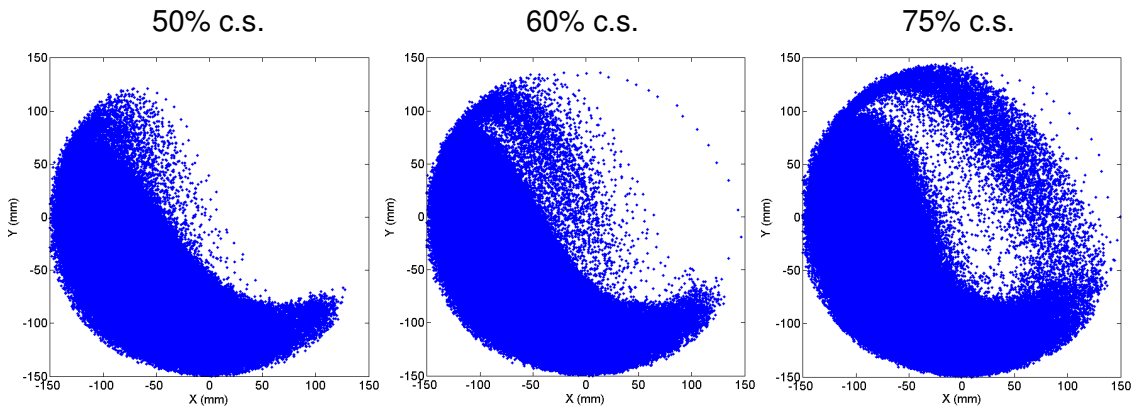

Figure 5. 1 – Superposition of the tracer's coordinates for 50, 60 and 75% critical speed.

Figure 5.2 (left) shows the location probability distributions that were obtained for the tests at 50, 60 and 75% of the critical mill speed. It is important to remember that the location probability gives the time spent by the tracer in a particular mill region. In the color diagram, presented in Figure 5.2, the red hue indicates the region with higher value of location probability and the blue hue a lower probability. As can be seen, the higher location probability is in the bean like shape, marked by light blue, yellow and red hue. Those plots give an indication of the region of the Centre of Circulation (CoC), point around which all particles circulate, marked by the red hue. In its vicinity, the

tracer moves more slowly, increasing the time spent in the same cell and its location probability, marked in the plots by a red hue in the bulk charge. The region above the bean like shape, marked by a blue hue, is mostly the cataracting region, indicating that this region plays a smaller role on the power draw, due to its minor location probability, as will be discussed as follows.

Another interesting feature that can be noticed in the location probability plot is thin blue region, under the bean like shape, in the periphery. This is due to the presence of the lifters. There are always particles in the region between them; however, the lifters reduce their mobility making it more difficult for the tracer to occupy it.

Similar plots can be graphed for the velocity profile in the mill, as shown in Figure 5.2 (right). The charge velocity profile was determined by averaging each absolute velocity registered for the tracer in the cells. The equilibrium surface was evident and marked by a dark blue hue, in the velocity plot. This surface separates the ascending en-masse charge (under the surface) from the descending charge (above the surface), making it a region of slower movement. In contrast, the red hue in the velocity plot indicates the region where the particles are being projected, the cataracting region. These plots confirm that the cataracting behavior is more prominent with increasing mill speed.

Figure 5.3 reproduces the spatial plots in the form of particle distributions along the two transversal axes, indicating the proportion of locations registered along the axes, in relation to the total number of registered positions. Note that the center of the axis was defined at the mill center. These distributions revealed a similar trend for the three rotational speeds. However, as expected and can be seen by the comparisons, as the speed increases the particles tend to move to the periphery of the mill. In the horizontal axis, the peak height increases with increasing mill speed, indicating a larger fraction of particles near the periphery of the mill. In contrast, in the center of the mill the fraction of particles decreases with increasing mill speed.

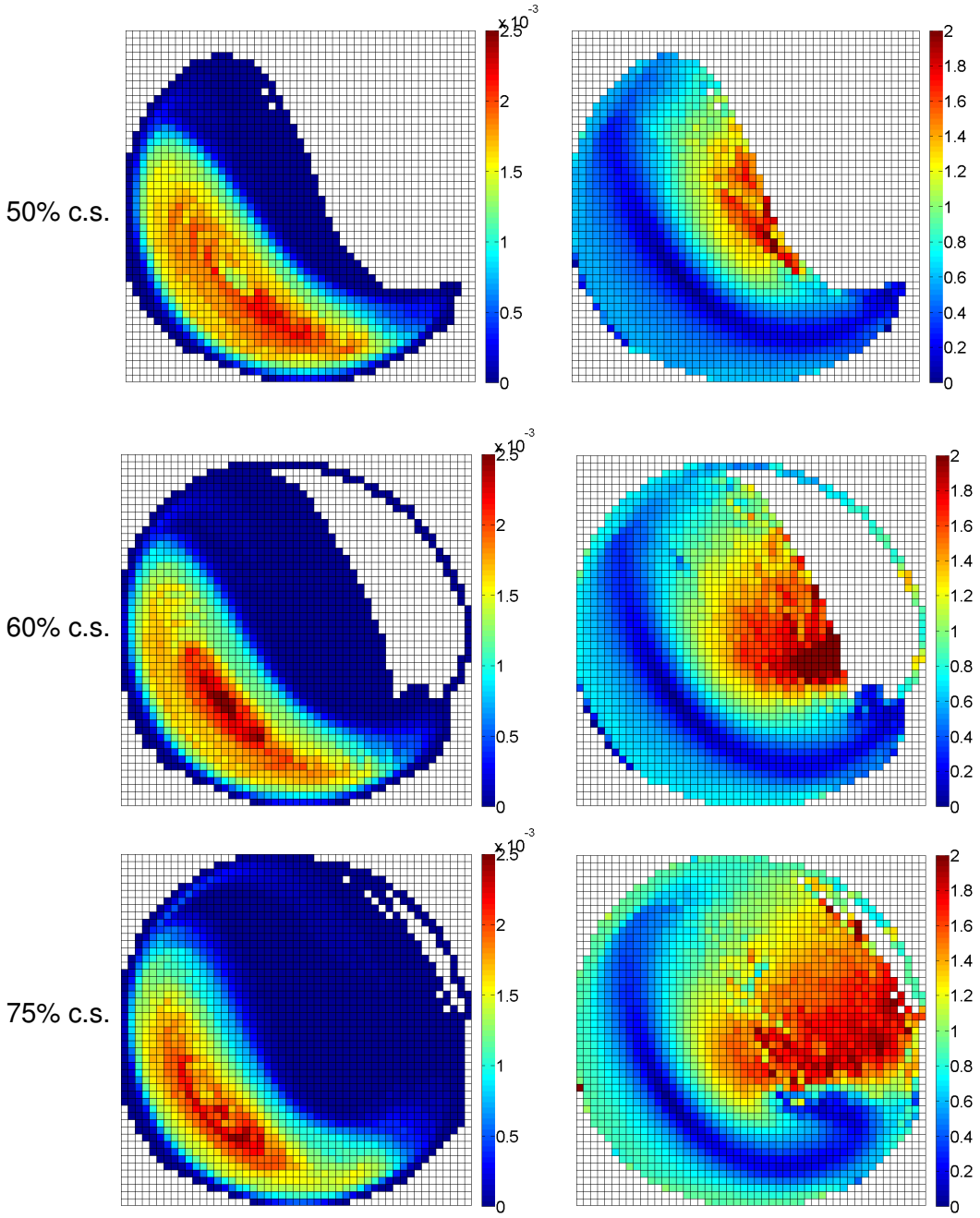

Figure 5. 2 – Spatial plots of location probability (left) and absolute velocity [m/s] (right) for 50, 60 and 75% critical speed.

In the vertical axis, however, the fraction of particles, in the peak region, decreases with increasing mill speed, with fewer particles in the lower section of the mill, indicating that they are lifted more (Figure 5.3).

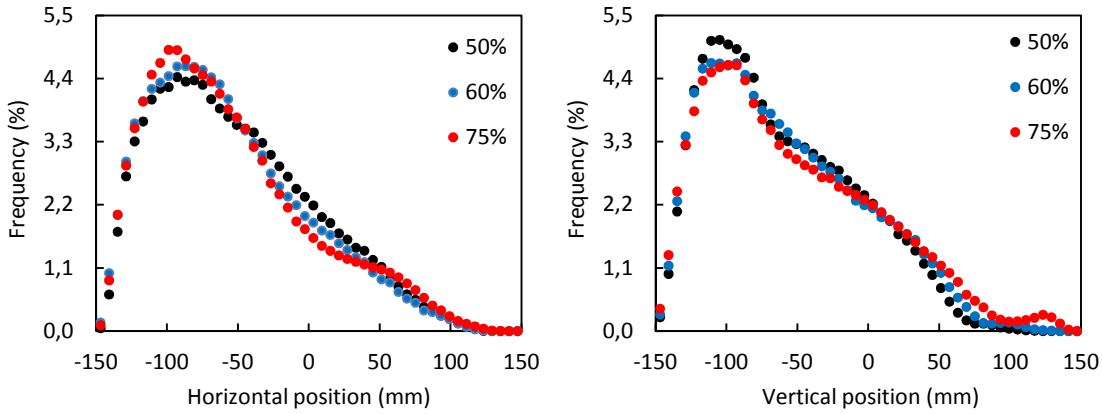

Figure 5. 3 – Particle distributions in X and Y directions.

Figure 5.4 shows the velocity distributions determined for the three tested conditions. As can be seen, the largest percentage of absolute velocity calculated is at the mill rotational speed, this is expected since the en masse charge, part of the charge being lifted near the periphery, tends to rise in conjunction with the mill shell. Comparing the curves for the three conditions, as the mill speed increases a larger frequency of absolute velocities registered is above the mill rotational speed. This happens due to the cataracting regime being more prominent under these conditions. Curiously, for the test at 75% c.s. nearly no particle velocities were higher than 2.5 times the mill speed, in contrast to the two other mill speeds.

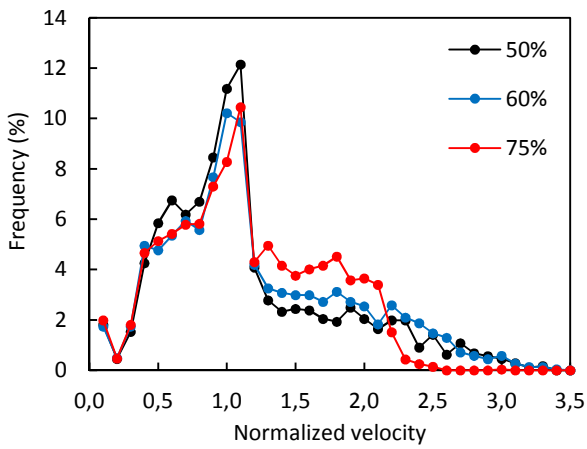

Figure 5. 4 – Distributions of velocity normalized by mill speed for PEPT data.

The power drawn by the mill and the error bars were calculated following the methodology described in section 4.2, using the PEPT data, and compared with the

values measured by the torque sensor attached to the mill apparatus, as shown in the bar graph in Figure 5.5. Values determined from PEPT data were found to be in good agreement with measurements, although marginally higher for 50 and 60% of critical speed. Since the method used to calculate the power is based on individual properties of every cell on the 50x50 grid, spatial distributions could be plotted to examine significant areas that contributed to the charge power draw, as presented in Figure 5.6.

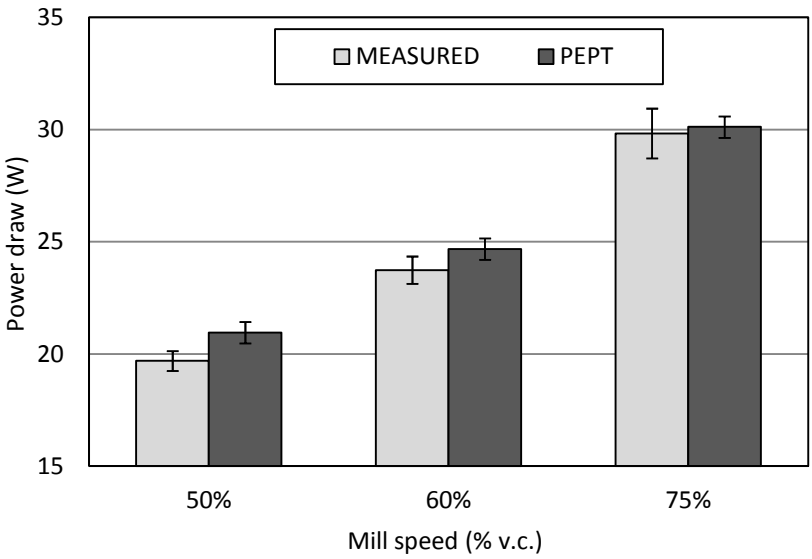

Figure 5. 5 – Comparison between power draw that was measured and estimated from PEPT.

The plots indicate that the bulk charge represents the higher contribution to the mill power draw, with negligible power being drawn by the cataracting region, above the free surface, in accordance with Morrel (1996) predictions. Two zones contribute significantly to the power draw (Figure 5.6), marked by a red hue and indicated as (1) and (2). The blue band dividing zones (1) and (2), coinciding with the equilibrium surface of the charge, has a lower contribution due to the lower velocity and, in consequence, lower angular velocity. The zone (1), near the periphery, is the rising en masse, and in this region high power draw were a consequence of the lifting action of the mill, where most of the work was done towards counteracting the effects of gravity. The zone (2) is the in cascading region, where the particles are sliding down to the charge toe. Here, energy is mainly consumed in counteracting the slip action of cascading charge. These two zones combine high particle density with high angular velocity, resulting in high power consumption. The cataracting region, although having higher velocity, has a low particle density which reduces its influence on the power.

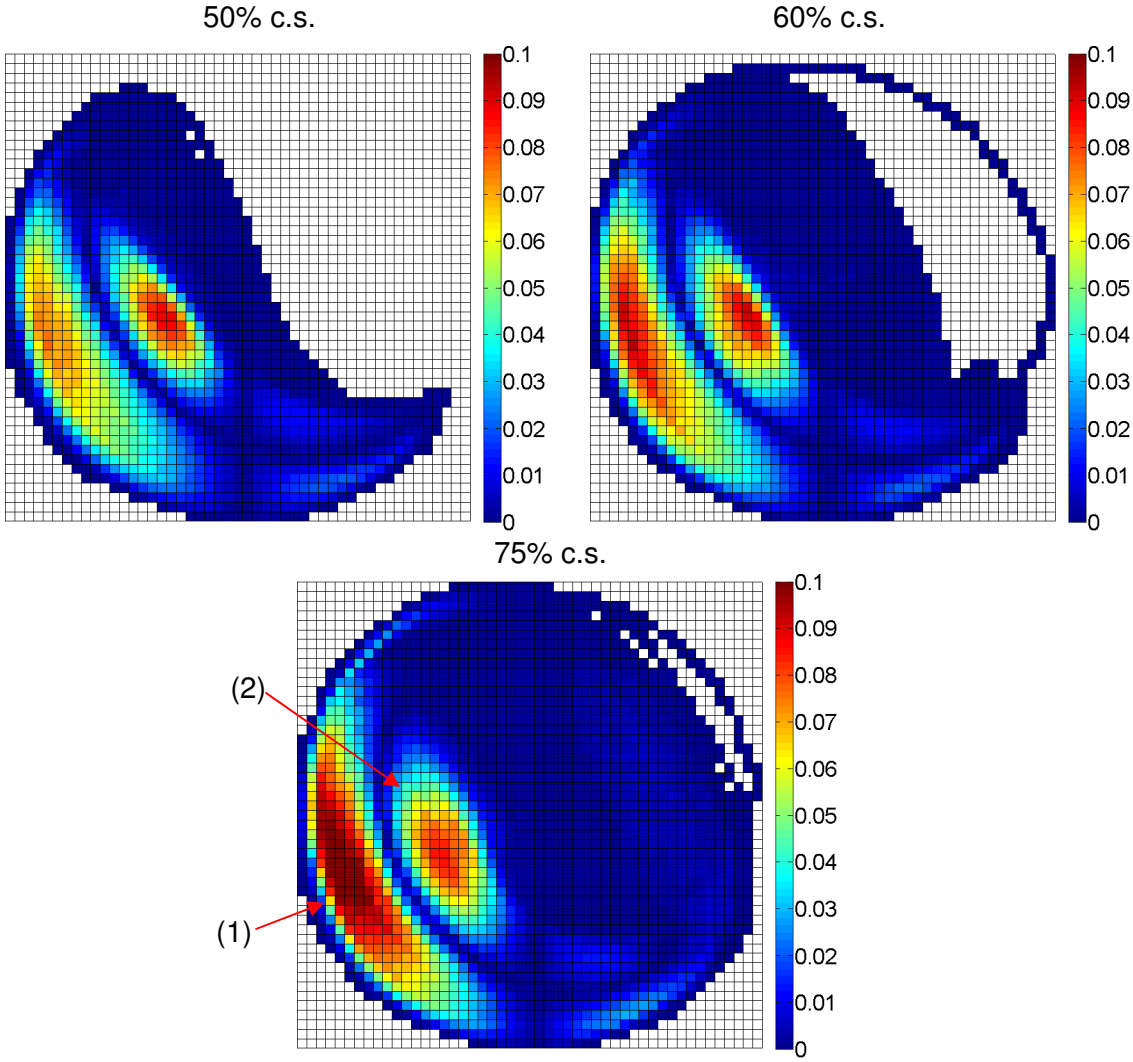

Figure 5. 6 – Spatial power draw distribution [W] for 50, 60 and 75% of mill critical speed.

Figure 5.6 demonstrated that with increase in mill speed, the power draw in zone (1) increases, marked by a more intense red hue. At higher speeds, more particles are pressed against the mill shell, as verified in Figure 5.3, due to the higher location probability. According to Morrel (1996), increasing the mill speed elevates the charge shoulder height and the energy consumption to lift the particles.

5.2. Validation of the ergodic hypothesis

The main assumption underpinning the use of PEPT in determining characteristics of the whole charge is that the system is ergodic. In short, ergodicity refers to the assumption that the time average of a single element of a system can be used to determine the ensemble average (Oliveira & Werlang 2007). With that in mind, a DEM simulation was conducted for one hour of simulated time, emulating the PEPT experiment, in which the motion data of a single particle was extracted in order to test this assumption. The material and contact parameters applied to the simulation were chosen based on a previous work done by Bbosa (2012). The simulation was conducted at 75% of mill critical speed and only a 50 mm section, ten times the particle size, in the middle of the mill was simulated in the sense of reducing the total number of particles and the time spent by the simulation. Three one-hour simulated time particles were chosen at random and its movements treated as PEPT data. The applied contact parameter values were not important since ergodicity is a statistical property of the mechanical system and not of the material. Besides, both parameters, for the single particles and the whole charge, were the same.

Figure 5.7 presents a comparison of the spatial plot of the absolute velocity and power draw distributions for the three single particles and for whole charge. From the spatial plots, it can be qualitatively observed that the motion registered of the single particles, for a long period of time, and the motion of the whole charge, for a few seconds, are very similar.

For a quantitative analysis, the power draw, distributions of particles along horizontal axis and of velocity were compared. The power draw calculated from the single particles and for the whole charge of particles is presented in Table 5.1. The distribution of particles along the X direction, in Figure 5.8 (left), and the distribution of velocity, normalized by the mill shell linear speed, in Figure 5.8 (right), indicate that the ergodic hypothesis holds valid for the tumbling mill dynamic system.

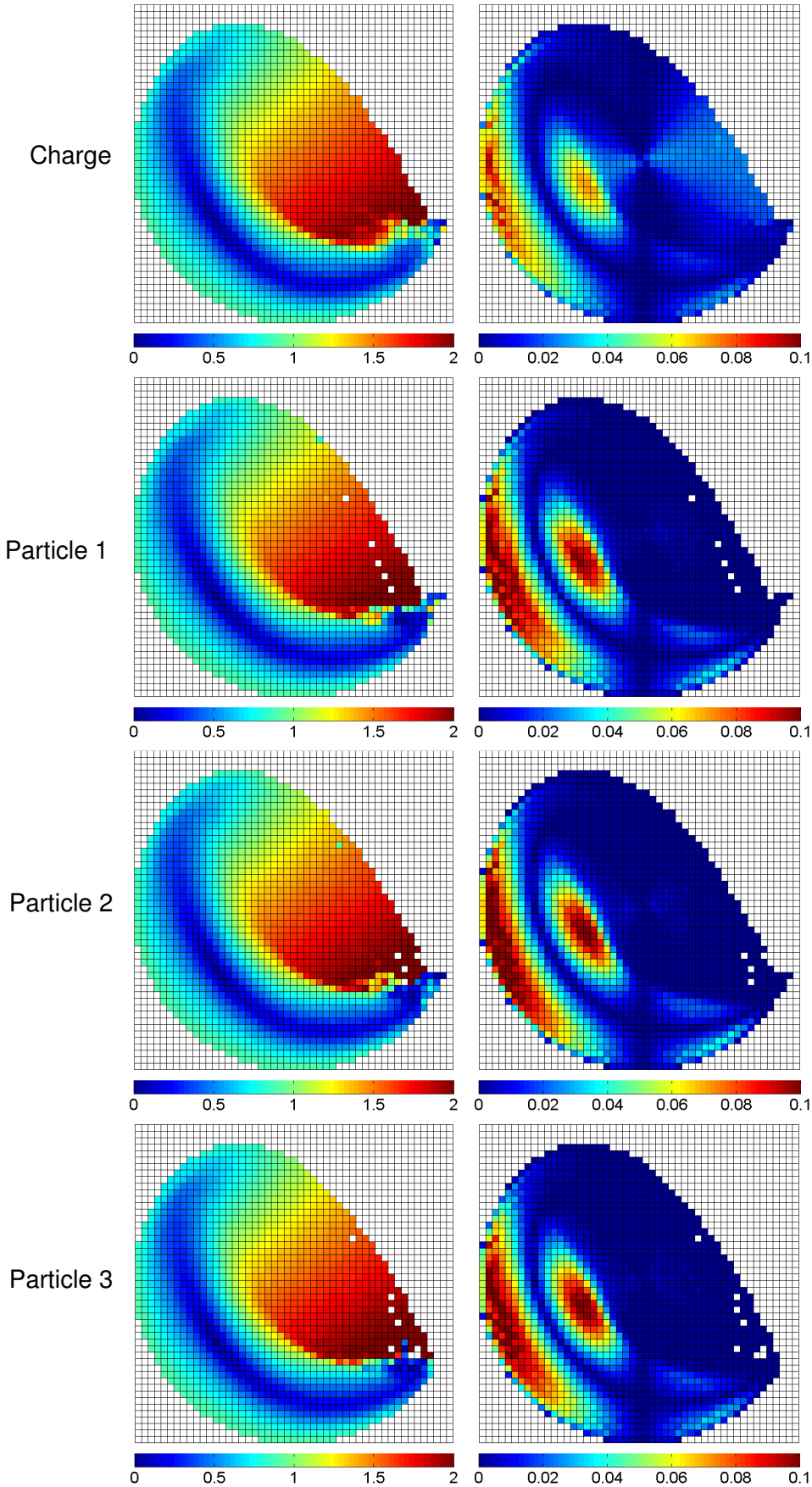

Figure 5. 7 – Spatial absolute velocity [m/s] (left) and power draw [W] (right) for the single particles and for the whole charge.

Table 5. 1 – Power draw [W] calculated for the whole charge of particles and for the single particles.

Charge	Particle 1	Particle 2	Particle 3
29.5	29.8	30.5	29.7

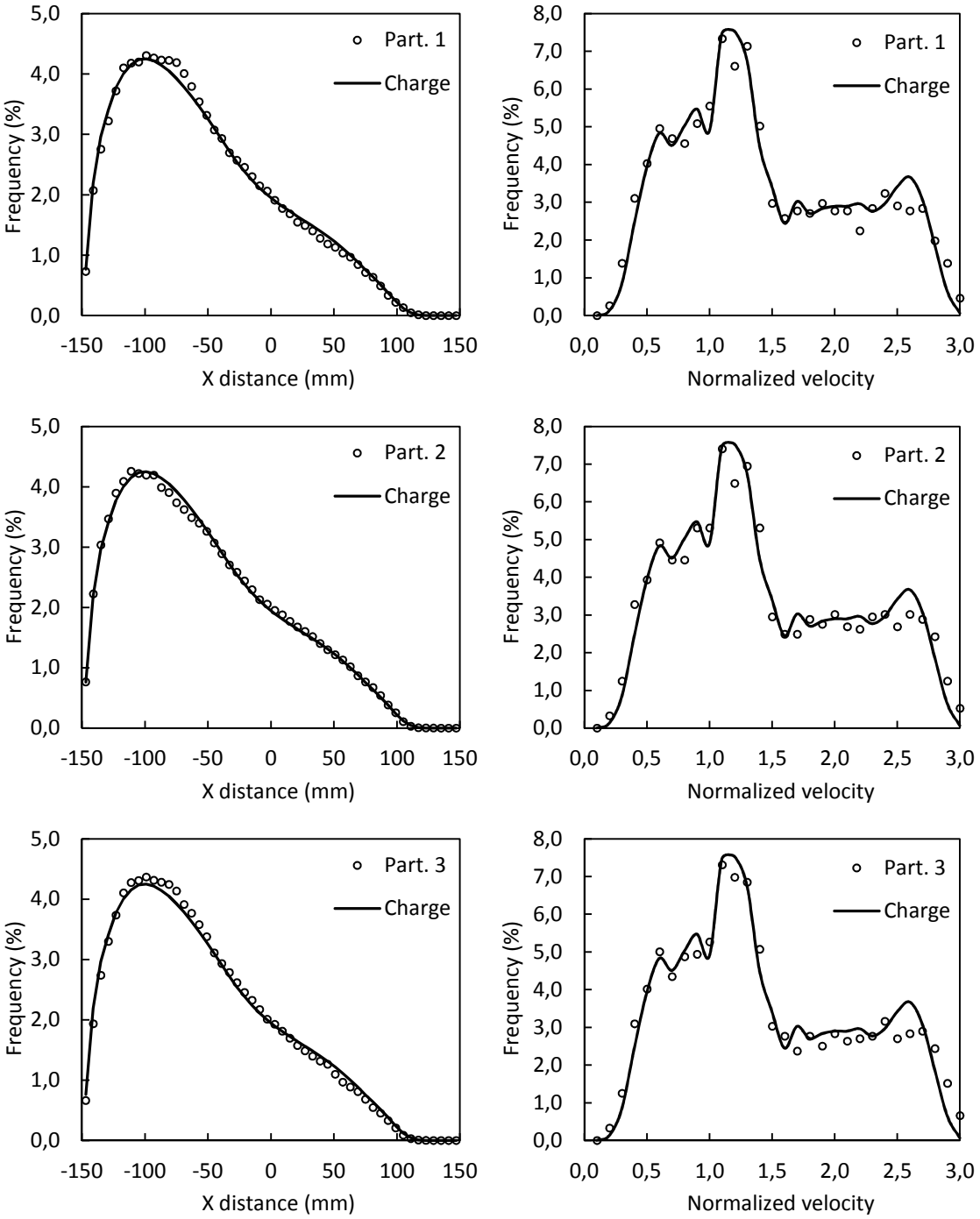

Figure 5. 8 – Comparison of the particle and velocity distribution of a single particle treated as PEPT, and the mill charge, at 60% critical speed.

5.3. DEM parameters calibration

5.3.1. Preliminary design of DEM simulations experiments

As discussed, the estimation of the optimal contact parameters was made on the basis of the data from the test at 75% of mill critical speed. Table 4.1 presents the first design of simulation experiments along with the calculated power draw and the objective function values (OF). The minimum and maximum levels were 0.3 and 0.7, respectively, with the cases 9, 10 and 11 being the central points with level 0.5. Figure 5.9 presents a comparison of the objective function values for the design cases. The power draw values presented in Table 5.2 were calculated following the methodology developed by Bbosa et al. (2011), with equation 3.2.

Table 5. 2 – Preliminary fractional factorial design of DEM simulation experiments along with the calculated power draw and the objective function (OF) value.

Cases	CRPP	CFPP	CRPG	CFPG	OF	Power (W)
1	0.3	0.3	0.3	0.3	1.70	29.8
2	0.7	0.3	0.3	0.7	1.41	30.3
3	0.3	0.7	0.3	0.7	2.16	30.9
4	0.7	0.7	0.3	0.3	2.29	31.1
5	0.3	0.3	0.7	0.7	1.13	30.1
6	0.7	0.3	0.7	0.3	1.34	29.9
7	0.3	0.7	0.7	0.3	1.89	30.7
8	0.7	0.7	0.7	0.7	2.29	31.4
9	0.5	0.5	0.5	0.5	2.15	31.0
10	0.5	0.5	0.5	0.5	1.95	30.8
11	0.5	0.5	0.5	0.5	1.92	30.8

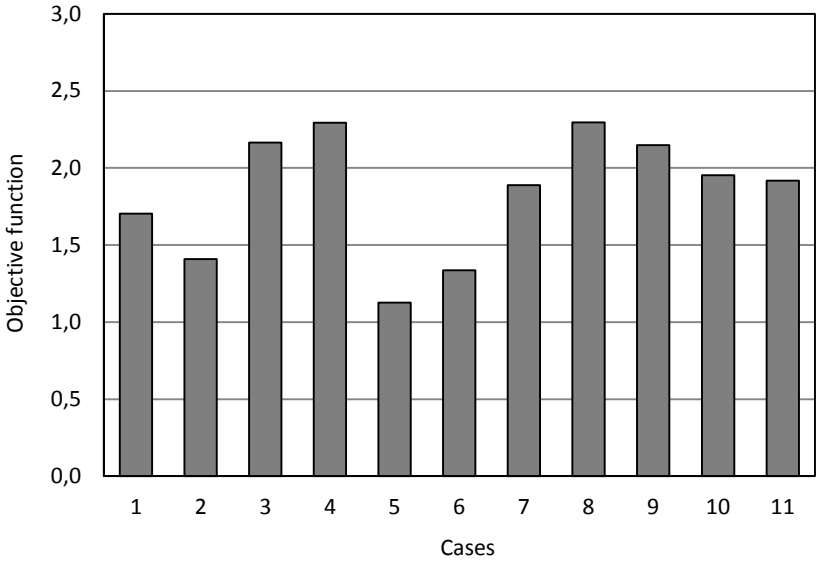

Figure 5. 9 – Objective function values for the preliminary design of DEM simulation experiments, conducted at 75% critical speed.

Figure 5.10 presents a comparison of the power draw found for the simulated cases with the one calculated using PEPT data. The error bar for the DEM simulations results are the standard deviation for the variation of calculated power over simulated time. At a first glance, considering the Power draw alone, as is common in other studies, some simulated cases stand out as having a set of parameters that could result in simulations that would approximately match the power draw estimated using PEPT. Examples are cases 1, 2, 5 and 6 that demonstrate how challenging it is to choose a particular set of contact parameters based on this criterion alone. The parameter value in common for these cases is the coefficient of friction particle-particle (CFPP), thus indicating its marked influence on the power draw. On the other hand, the objective function values, that also considers charge motion, indicates difference among them. The objective function value for case 5 is around 30% smaller than the one found for case 1, for example.

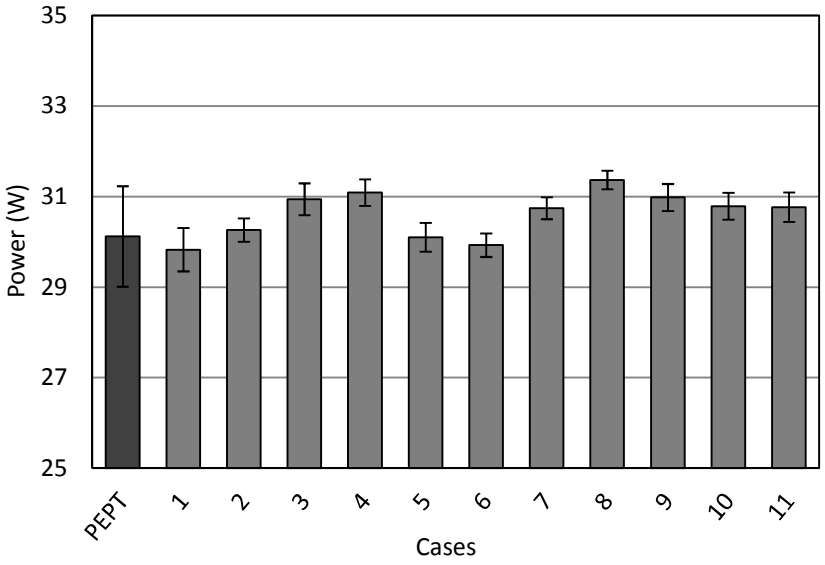

Figure 5. 10 – Power draw calculated for PEPT and DEM simulations in the preliminary design of simulation experiments.

With the results of the first batch of simulations, a statistical analysis of variance was carried out, using a 90% confidence level. Table 5.3 presents the analysis of variance results. The analysis showed the coefficient of friction particle-particle (CFPP) as the most significant variable for the objective function, also confirming what was indicated by the power draw comparison. As mentioned in section 3.2, van Nierop et al. (2001) showed that the power draw, and therefore the objective function used in this study, is dependent on the coefficient of friction applied, confirming the result of the analysis of variance. Figure 5.11 shows the relation of the power draw with the coefficient of friction for a 2D mill DEM simulation, extracted from the work done by van Nierop et al. (2001) and a similar analysis done for the PEPT mill in a preliminary assessment on the influence of the parameter. In both analyses the other parameters were kept constant. The high influence of the inter particle friction is expected once the tracer expends most of the time in the en masse charge, region where the particles are in constant contact and tangential forces are dominant.

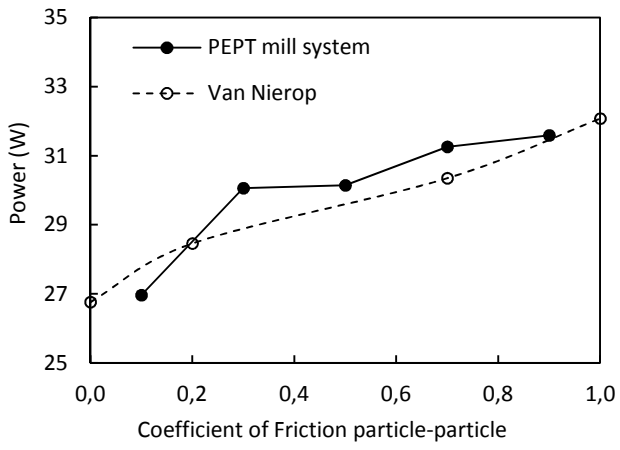

Figure 5.11 – Influence of the coefficient of friction on the power draw. Extracted from van Nierop et al. (2001), at 80% critical speed with 35% mill filling (dashed line) and the analysis done for the PEPT mill system, at 75% critical speed (full line).

A second significant variable is the coefficient of restitution particle-geometry (CRPG), although not as significant as the CFPP. The other two parameters, however, the coefficient of restitution particle-particle and of friction particle-geometry, had a negligible effect in the defined objective function.

The analysis of variance also indicated the presence of curvature for the objective function in the region of the first simulation plan, which suggests that its minimal value is in this region.

Table 5. 3 – Analysis of variance (ANOVA) for the preliminary design of simulation experiments.

	Degrees of freedom	Sum of squares	Mean squares	F-value	P-value
CRPP	1	0.03	0.03	0.73	0.497
CFPP	1	1.18	1.18	33.95	0.003
CRPG	1	0.11	0.11	3.08	0.187
CFPG	1	0.01	0.01	0.19	0.722
Curvature	1	0.12	0.12	3.32	0.128
Error	5	0.17	0.03		
Total		1.60			

The analysis of variance also indicated the presence of curvature for the objective function in the region of the first simulation plan, indicating that the minimal value might be within the design region. In Figure 5.12 is presented the objection function with the

variation of the contact parameters individually. It can be seen that the results of the analysis of variance were confirmed, with the coefficient of friction particle-particle (CFPP) resulting in the widest variation. Most likely the response of the objective function with the CFPP is responsible for the curvature detected by the ANOVA.

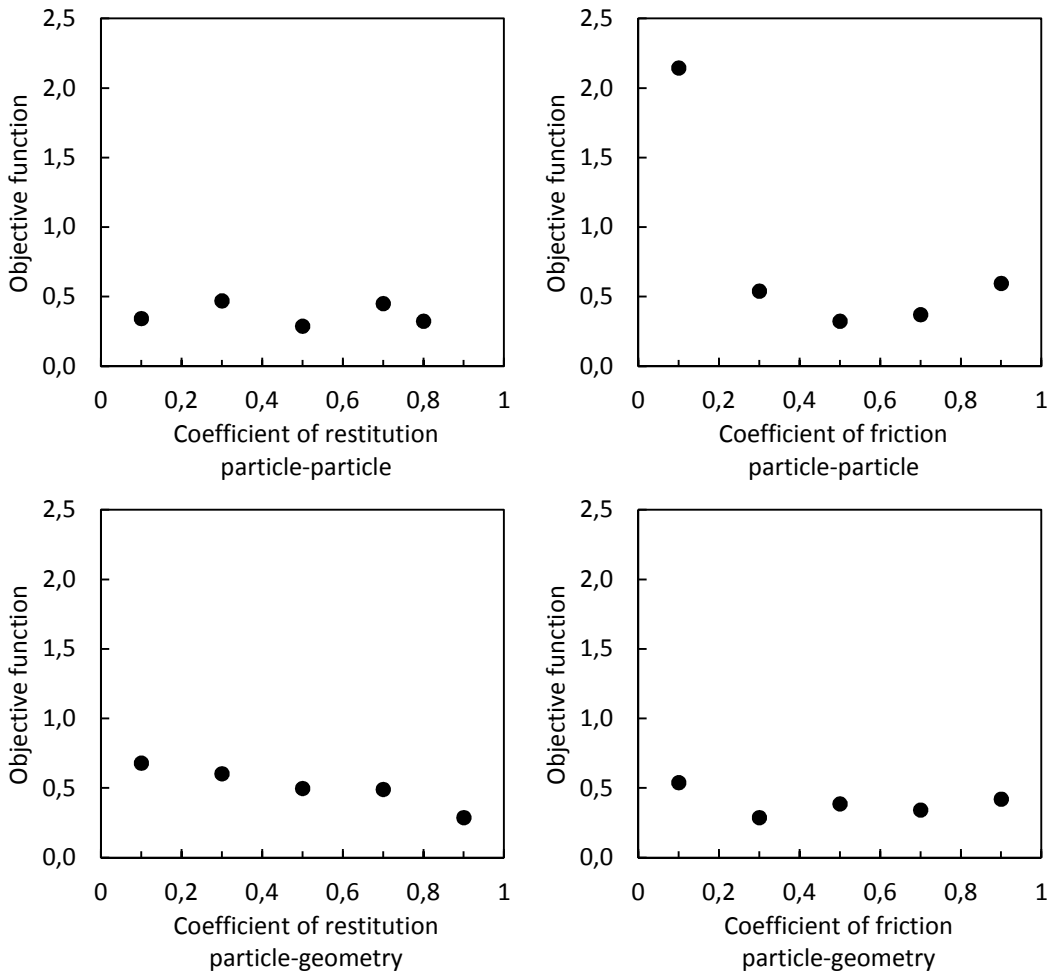

Figure 5.12 – Objective function results with the variation of the parameters individually.

5.3.2. Refined design of DEM simulation experiments

With the aim of reducing the number of variables for an additional, more complex, design of simulation experiments it was decided to fix the CRPP and CFPG to values of 0.8 and 0.3, respectively. These values were chosen based on a study done by González-Montellano et al. (2012), in which DEM contact parameters for glass beads against a polymeric surface were experimentally determined and presented values of 0.808 for the CRPP and 0.299 for the CFPG.

Appling the method of steepest descent to the first order model of the objective function designed from the first simulation design, it was determined that the optimal set of parameters was somewhere between the range [0.2 ; 0.4] for the CFPP and [0.53 ; 0.59] for the CRPG. A central composite design was created around the range of the parameters found and is presented in Table 5.4 along with the calculated power draw and the objective function values, also shown in Figure 5.12.

Table 5. 4 – Central composite design of DEM simulation for the CFPP and CRPG along with the calculated power draw and the objective function (OF) value.

Cases	CFPP	CRPG	OF	Power (W)
12	0.20	0.53	2.33	29.0
13	0.40	0.53	1.55	30.4
14	0.20	0.59	2.29	31.4
15	0.40	0.59	1.68	30.5
16	0.16	0.56	2.96	28.4
17	0.44	0.56	1.77	30.7
18	0.30	0.52	1.20	30.2
19	0.30	0.60	1.33	30.0
20	0.30	0.56	1.28	30.0
21	0.30	0.56	1.26	30.2
22	0.30	0.56	1.22	30.0
23	0.30	0.56	1.26	30.0
24	0.30	0.56	1.30	29.9

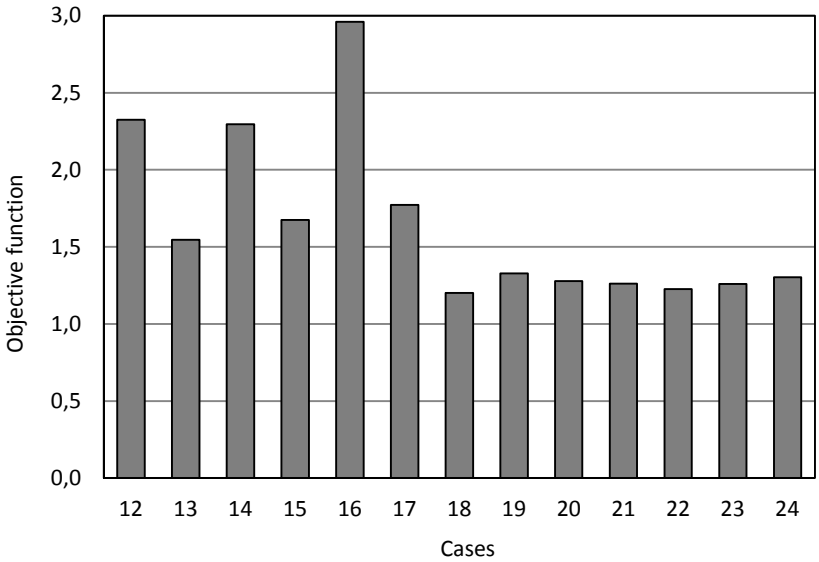

Figure 5. 12 – Objective function values for the refined design of DEM simulation experiments, for the mill operating at 75% critical speed.

From the second design of simulation experiments, a new statistical analysis of variance was conducted, using a 90% confidence level, considering not only the influence of the two parameters tested but also the quadratic terms for the parameters. Table 5.5 summarizes the analysis of variance results. It was found that the quadratic term of the CFPP presented even greater influence on the objective function than its linear term, reaffirming the importance of this parameter to the result of the simulation.

Table 5. 5 – Analysis of variance (ANOVA) for the second design of simulation experiments.

	DF	SS	MS	F	P
CFPP	1	1.19	1.19	147.30	0.000
CFPP²	1	2.39	2.39	297.61	0.000
CRPG	1	0.01	0.01	1.21	0.307
CRPG²	1	0.01	0.01	1.10	0.329
CFPP x CRPG	1	0.01	0.01	0.80	0.402
Error	7	0.06	0.01		
Total	12	3.66			

A statistical model was developed for the relationship between the objective function and the two contact parameters, CFPP and CRPG, and is given by

$$Obj.func. = 1.27 - 0.39 \cdot CFPP + 0.03 \cdot CRPG + 0.59 \cdot CFPP^2 + 0.04 \cdot CRPG^2 + 0.04 \cdot CFPP \cdot CRPG.$$

Figure 5.13 presents the response surface of the objective function, plotted applying the developed statistical model, in relation to the contact parameters CFPP and CRPG. From the statistical model an estimation of the optimal combinations of values for the CFPP and CRPG, by minimizing the objective function, that is, the difference between PEPT and DEM data. The estimated set of parameters were 0.34 and 0.55 for the CFPP and CRPG, respectively. Table 5.6 summarizes all calibrated parameters.

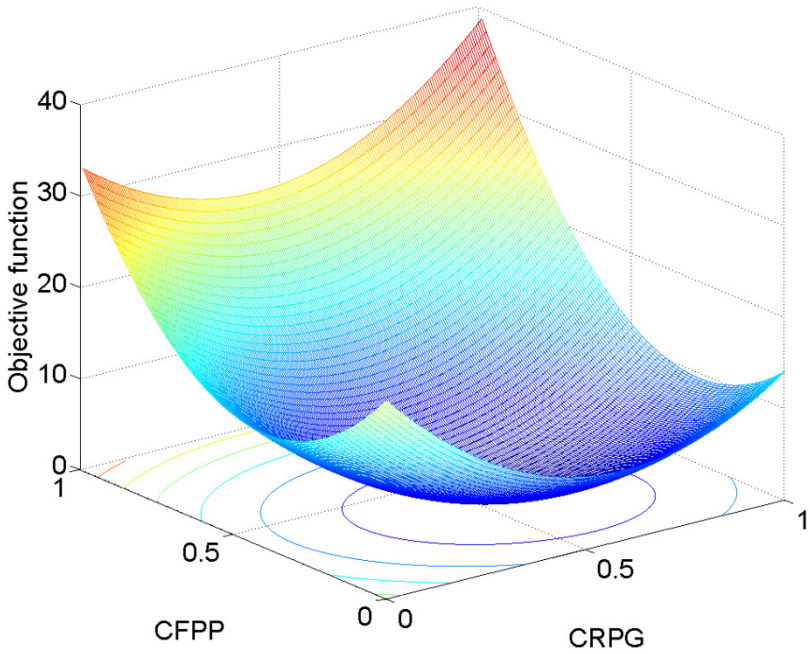

Figure 5. 13 – Response surface of the objective function in relation to the parameters CFPP and CRPG.

Table 5. 6 – Optimal set of contact parameters.

Contact parameter	Value
Coefficient of restitution particle-particle	0.80
Coefficient of friction particle-particle	0.34
Coefficient of restitution particle-geometry	0.55
Coefficient of friction particle-geometry	0.30

With the calibrated set of contact parameters, additional simulations were run in order to compare simulations with experimental results. Figure 5.14 presents the spatial power draw distributions for PEPT and DEM and a spatial plot of the difference (PEPT minus DEM). The power draw difference plotted in the figure indicated that the largest difference occurred along the periphery of the mill where DEM is marginally higher than those of PEPT. As explained previously, this difference is due to presence of the lifters, which reduce the particle mobility in this region making it more difficult for the tracer to occupy it. However, for DEM all the particles are tracked and are included in the power calculation, including the ones between lifters, resulting in this difference.

An additional discrepancy between the plots in Figure 5.14 (a) and (b) is in the cataracting region. In PEPT, particles appear to be projected farther than in the DEM simulation. That might be explained by the presence of end faces of the mill. Remembering that for the DEM simulations, only a slice of the mill was simulated with the aim of reducing computational time, removing the effect of the end faces. Nevertheless, considering the low particle density and low power draw in this region, this difference could be overlooked. Indeed, in Figure 5.14c it is demonstrated that this difference is nearly zero.

Regardless of the divergences mentioned above, it is safe to state that the DEM simulation, using the calibrated parameters is in very good agreement with the PEPT results. The spatial power draw distributions take into account a series of variables, such as location probability, linear and angular velocity, enabling in case of inadequate set of parameters occurrence discrepancies in those properties and consequently in the regions of high power. Nonetheless both plots display a consistent trend in the high power areas, as is also confirmed by the difference plot in Figure 5.14c. The total power draw for PEPT and DEM are compared in Figure 5.15, showing an error of around 1% between both power values, adding confidence to the calibrated parameters. The marginally higher power draw for DEM data, might be explained by the difference in the peripheral region, left side of the plots (Figure 5.14c), on which DEM register higher power draw.

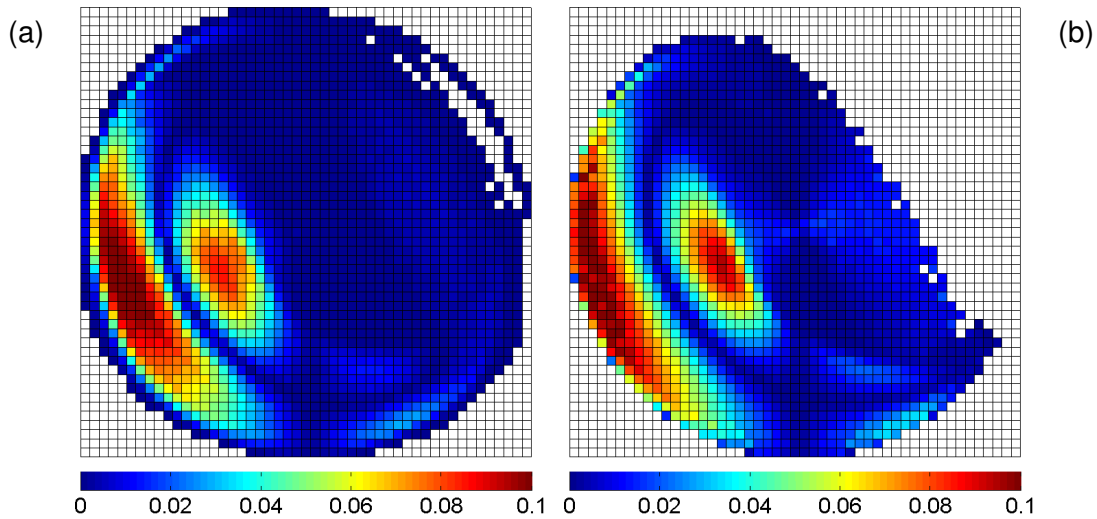

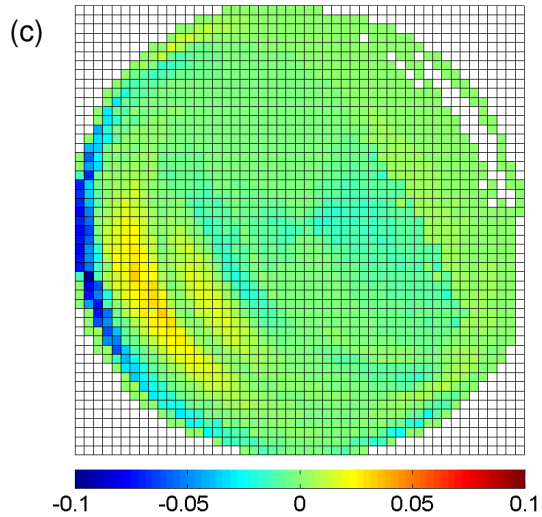

Figure 5. 14 – Spatial power distribution [W] for (a) PEPT, (b) DEM with calibrated parameters and (c) difference PEPT - DEM.

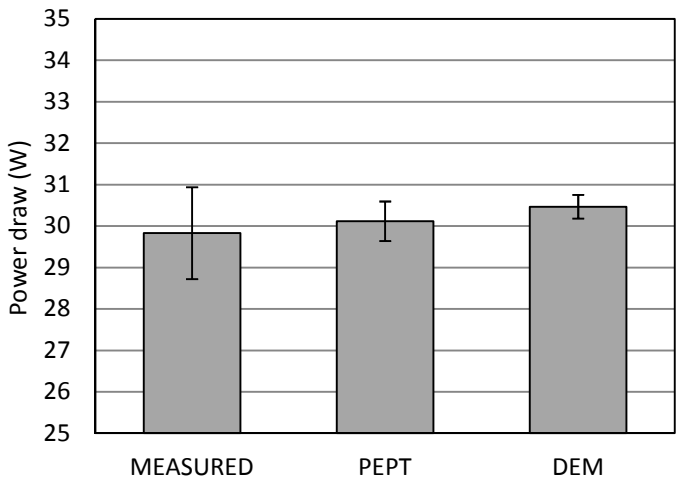

Figure 5. 15 – Power draw measured and calculated using PEPT and DEM simulations with the calibrated parameters at 75% critical speed.

Examining the particle and velocity distributions, shown in Figure 5.16 for PEPT and DEM using the calibrated parameters, the agreement between them becomes evident. Considering the particle distribution (Figure 5.16a), PEPT and DEM curves showed similar trends, however, with a small deviation. The PEPT distribution presented a peak, at around the position -100 mm, higher than the DEM distribution, with a difference of about 0.5% for the frequency of particles in this position, indicating that the PEPT system kept the particles nearer to the periphery of the mill than DEM. However, if we examine the cumulative frequency of the particle distribution, in Figure 5.16c, the good agreement among the curves becomes evident, demonstrating the overall similarity of the distribution of charge along the mill transversal plane.

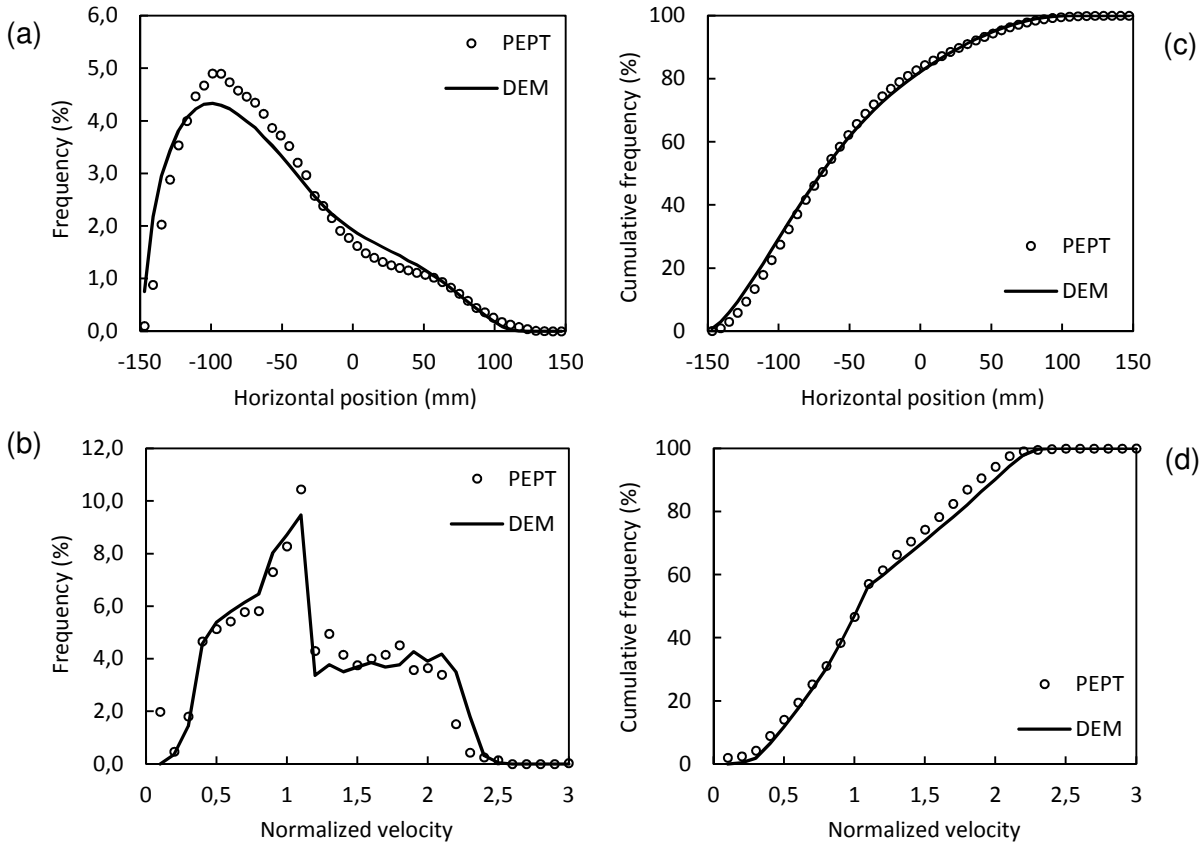

Figure 5. 16 – Distributions of (a) particle in the horizontal direction, of (b) velocity and their cumulative frequency (c and d), at 75% critical speed.

Figure 5.16b and d showed that the distribution of absolute velocity performed by the particles in both systems is in very good agreement, especially looking at the data in cumulative frequency form (Figure 5.16d). Both curves confirmed that the velocity in which the particles spend more time is near the mill speed. As mentioned in section 5.1 and looking at Figure 5.4, the experiment at 75% critical speed did not register absolute velocities above 2.5 times the mill rotational velocity. Still the DEM simulation, using the calibrated parameters, was capable of reproducing this result.

5.4. DEM parameters validation

Once the optimal set of parameters has been identified, calibrated using PEPT data for the test at 75% critical speed, they could be applied to different milling conditions. In

order to validate the parameters found, DEM simulations of the PEPT experiments at 50 and 60% critical speed were conducted using these parameters. Figure 5.17 presents the power draw measured, along with the values calculated for PEPT and DEM data, using the optimal parameters, for 50, 60 and 75% critical speed It can be observed that simulations carried out using the parameters calibrated at 75% critical speed were capable of appropriately predicting the power draw calculated from PEPT data in different conditions.

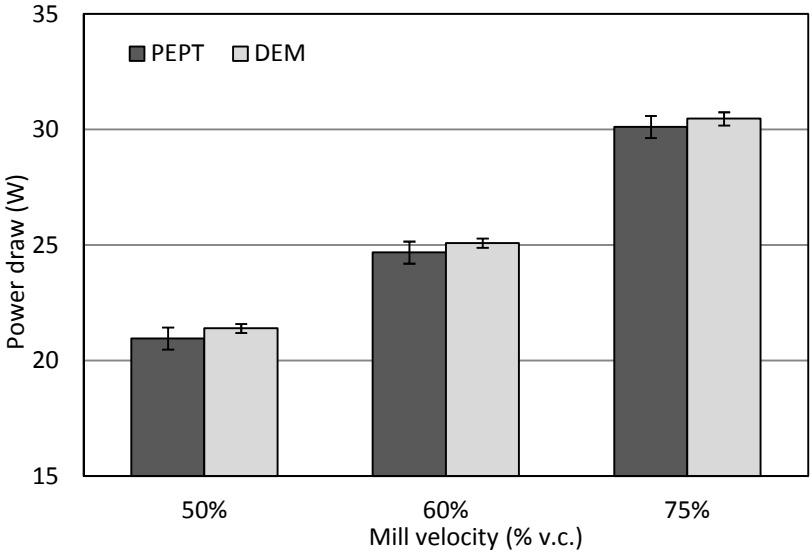

Figure 5. 17 – Power draw calculated using PEPT data and DEM simulations with the calibrated parameters.

In Figure 5.18, the particle distributions and its cumulative form from PEPT data and DEM simulations, using the calibrated parameters, are compared for the three tested mill speeds. Looking at cumulative distribution, it can stated that simulation with calibrated parameters resulted in good agreement with PEPT data for the three mill speeds. However, the discrete distribution, Figure 5.18 (left), reveals discrepancies between the two techniques. The DEM simulations followed the same trend as PEPT, but the peak of the three curves, at around position -100 mm, were not as high as for PEPT, indicating that the charge during the PEPT experiments was concentrated farther from the mill center, to the left, than in the DEM simulations.

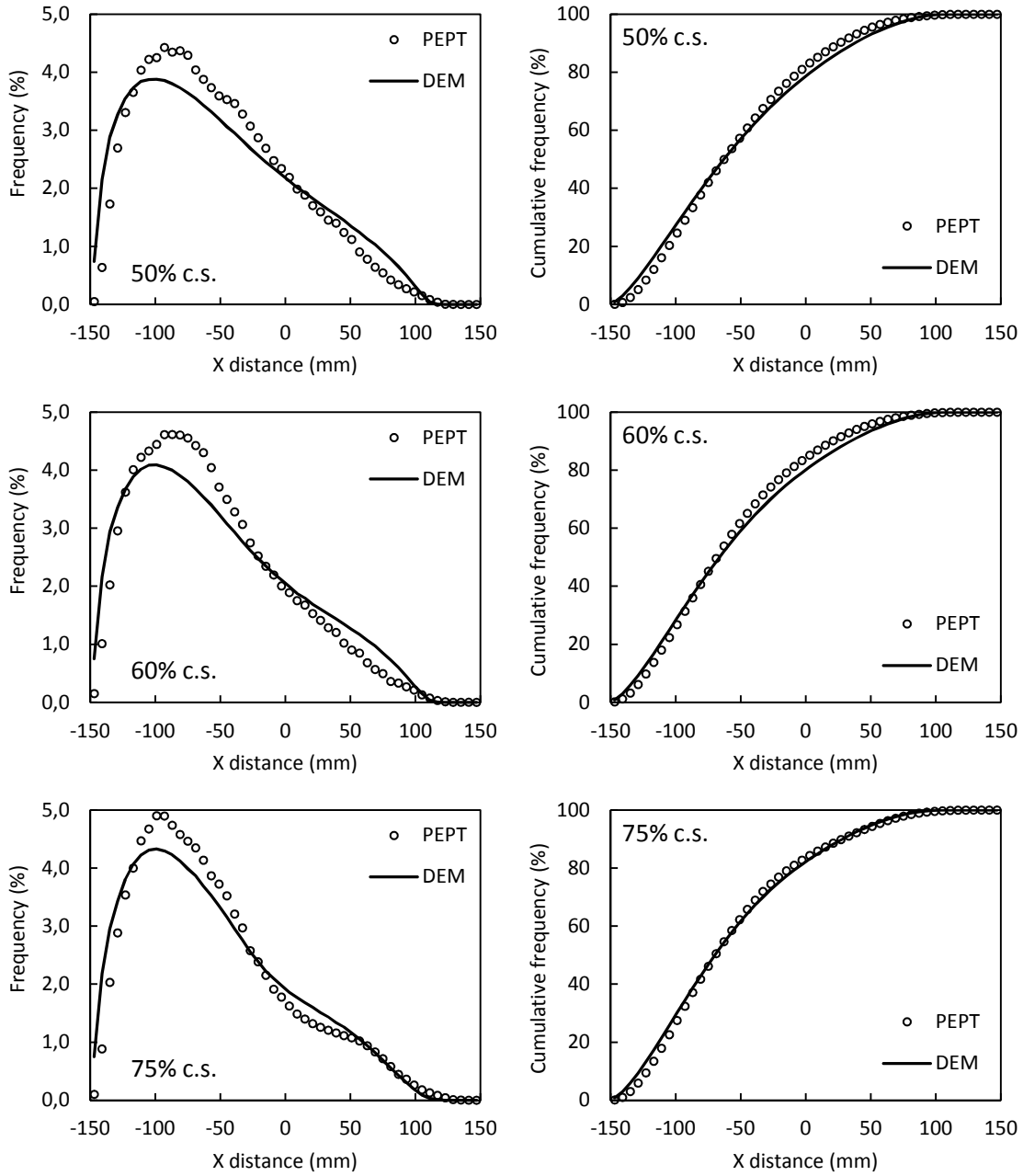

Figure 5. 18 – Particle distributions in X direction for PEPT and DEM simulations with the calibrated parameters.

In Figure 5.19 it is compared the velocity distribution normalized by the mill rotational velocity and its cumulative form for PEPT and DEM data. From the plots it is possible to notice that the PEPT and DEM distributions followed the same trends, with a peak at the mill rotational speed, in fact, around 50% of the particle are between 0.5 to 1 times the mill speed for three conditions. Although both distributions for PEPT and DEM, at 75% critical speed, were in very good agreement, discrepancies appeared at the other two tests. At 50 and 60% critical speed, DEM simulations presented higher frequencies for lower than the 1 time mill rotational velocity. These discrepancies indicate the need for caution when simulating conditions too far from the one used in calibration.

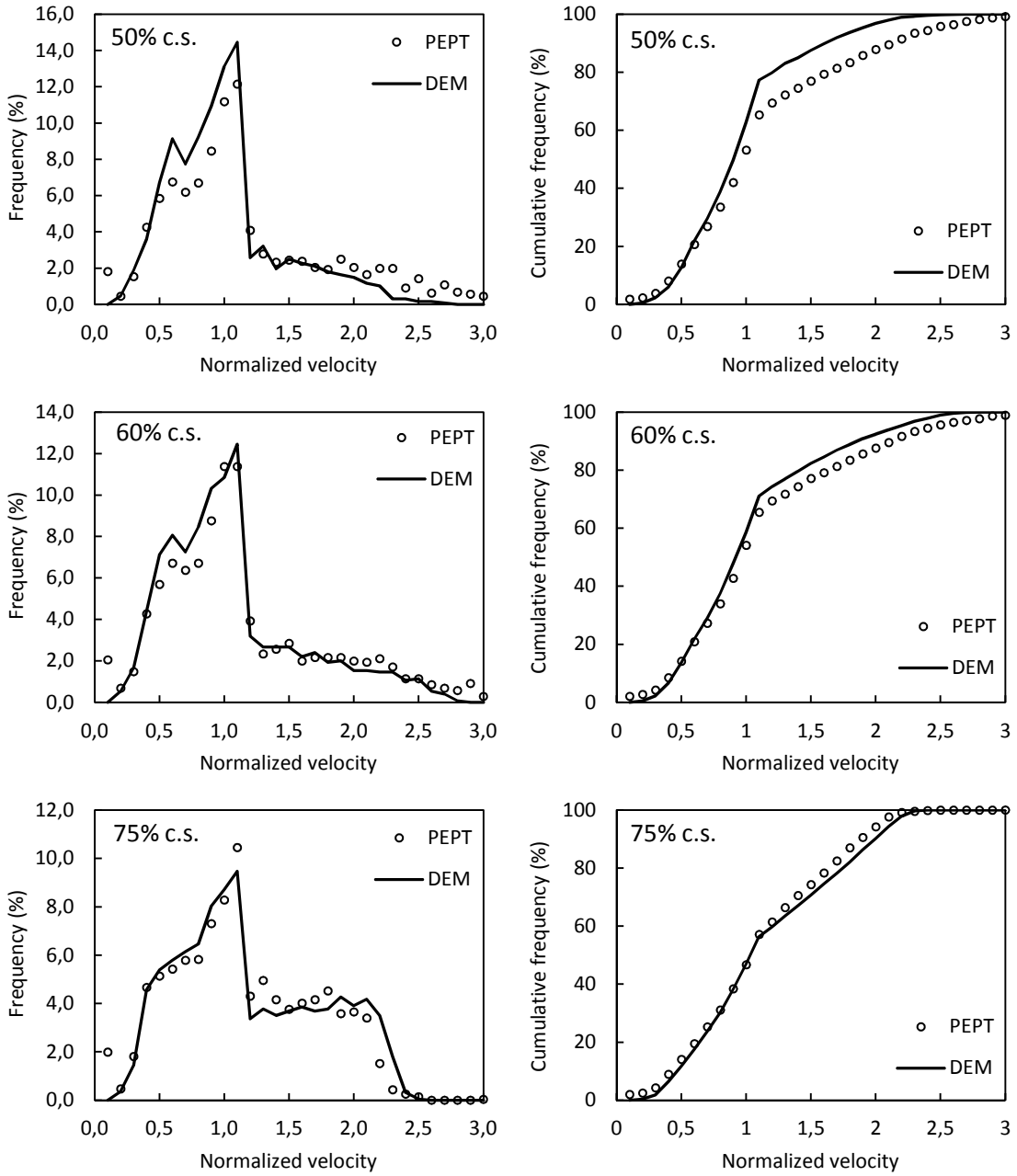

Figure 5. 20 – Velocity distributions normalized by the mill speed for PEPT and DEM simulations with the calibrated parameters.

6. Conclusions

The scope of this work was guided on the hypothesis the effect of operational conditions on charge movement in a tumbling mill could be quantified using data from PEPT. Evidence on the veracity of this hypothesis was obtained through DEM simulation emulating the PEPT experiment.

PEPT experiments were then conducted using dry glass bead charge of 5 mm in a laboratory scale tumbling mill, in the mill speeds of 50, 60 and 75% of the critical speed. The statistical properties from these tests were used for calibration and validation of DEM contact parameters, carried out using an identical mill geometry and charge. Data from these two approaches was used to determine and comparer the charge power, mass distribution throughout the mill projection plane and velocity distribution.

The assumed hypothesis was confirmed based on the following conclusions:

- Power draw values calculated from PEPT data were similar with power measured directly during the experiments, although marginally higher for 50 and 60% of critical speed.
- DEM simulation tracking the movement of a single particle for one hour of simulated time resulted in very good agreement between single particle and complete charge when comparing spatial plots of absolute velocity and power draw.
- The similarity for the particle distribution along the mill projection plane and normalized velocity distribution were an additional evidence of the validity of the ergodic hypothesis.

On the influence of parameters, it was observed that the coefficient of friction between grinding media in DEM has a great influence on the power consumption, which is expected considering that for condition with mill speed under 100% c.s., for the largest part of the time, particles are only in contact with other particles. Additionally, the adopted method for determining power draw looks in the point of view of the particles, instead of the mill geometry, revealing the influence of particle interaction. On the other hand, the coefficient of friction between particles and the mill shell was found irrelevant to charge motion, what is also expected once most of the particles in direct contact with the mill walls hardly slip and are dragged, by action of the lifters, along with it.

Although the contact parameters found by the calibration responded satisfactorily in the three tested conditions and overall tendencies for particle and velocity distribution were

similar, some discrepancies were verified. It is also important to notice that no set of parameters tested was able compare perfectly to the PEPT distributions, being the ones chosen as optimal the closest approximation. Even so, the optimal set of contact parameters, found by the calibration can provide good approximation for different milling conditions, such as different mill speed, filling, geometry and particle size distribution.

7. Future work

The experimental work and simulations done for this study were performed at dry, what is unusual in the mineral industry. Further studies assessing the influence of water and slurry on charge motion should be conducted. Figure 7.1 presents a comparison of PEPT tests at dry and using slurry of 5% of solid, both at 75% critical speed, with monosize 5 mm particles. The spatial velocity and power plots have not presented any significant difference. The equilibrium surfaces, blue hue band in the velocity plot, are nearly in the same position. In the power plots, the high power regions are also about the same size and in the same location. The total power draw, however, presented the main difference between the tests, being 30.1 and 26.0 W for the dry and wet tests, respectively. A 46% drop on power consumption just by adding slurry.

The DEM simulations of the wet test is still a challenge. More studies would have to be done in order to manipulate the parameters to compensate the absence of the liquid phase.

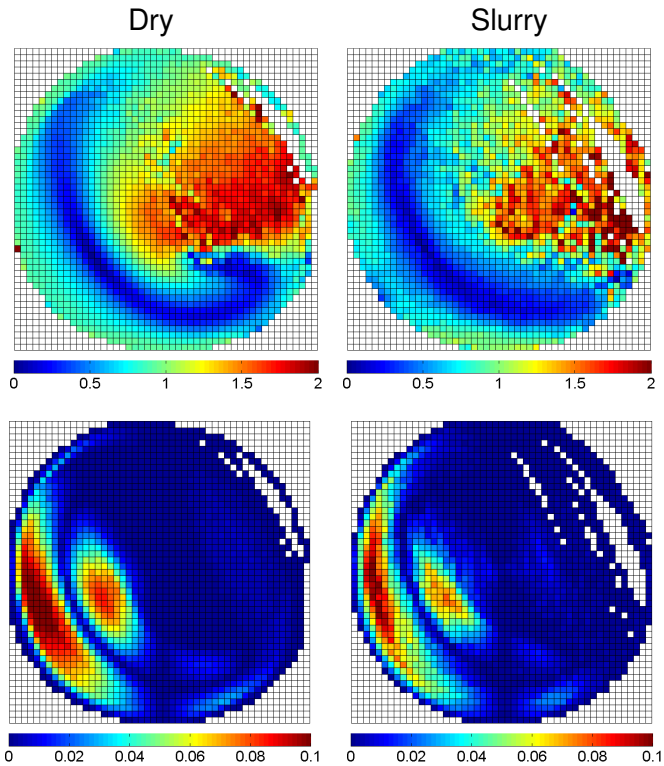

Figure 7.1 - Spatial absolute velocity [m/s] (up) and power draw [W] (down) at 75% critical speed with 31.3% mill filling of monosize 5 mm glass beads, at dry (left) and with slurry of 5% solid.

8. References

Austin, L.G., Concha, F., 1994. *Diseño y simulación de circuitos de molienda y clasificacion* (Vol. 1). Universidad Técnica Federico Santa María Ediciones.

Baumann, G., Janosi, I.M., Wolf, D.E., 1994. Particle Trajectories and Segregation in a Two-Dimensional Rotating Drum. *Europhysics Letters*, 27(3), pp. 203 – 208.

Bbosa, L.S., Govender, I., Mainza, A., Powell, M., Plint, N., 2012. Comparing Power Draw Predictions in Experimental Scale Tumbling Mills Using PEPT and DEM. *XXVI International Mineral Processing Congress (IMPC)* 2012, pp.2750–2760.

Bbosa, L.S., Govender, I., Mainza. A., Powell, M.S., 2011. Power draw estimations in experimental tumbling mills using PEPT. *Minerals Engineering*, 24(3-4), pp.319–324.

Bond, F.C., 1960. Crushing and grinding calculations. *British Chemical Engineering*, 6, pp.378–391.

Carvalho, R.M., Tavares, L.M., 2013. Predicting the effect of operating and design variables on breakage rates using the mechanistic ball mill model. *Minerals Engineering*, 43-44, pp.91–101.

Cleary, P.W., 1998. Predicting charge motion, power draw, segregation and wear in ball mills using discrete element methods. *Minerals Engineering*, 11, pp.1061–1080.

Cleary, P.W., 2015. Prediction of coupled particle and fluid flows using DEM and SPH. *Minerals Engineering*, 73, pp.85–99.

Cundall, P.A., Strack, O.D.L., 1979. A discrete numerical model for granular assemblies. *Géotechnique*, 29(1), pp.47–65.

Curry, J.A., Ismay, M.J.L., Jameson, G.J., 2014. Mine operating costs and the potential impacts of energy and grinding. *Minerals Engineering*, 56, pp.70–80.

Dong, H., Moys, M.H., 2003. Load behavior and mill power. *International Journal of Mineral Processing*, 69, pp.11–28.

Etsion, I., 2010. Revisiting the Cattaneo–Mindlin Concept of Interfacial Slip in Tangentially Loaded Compliant Bodies. *Journal of Tribology*, 132(2).

Fuerstenau, D.W., Abouzeid, A.Z., 2002. The energy efficiency of ball milling in comminution. *International Journal of Mineral Processing*, 67, pp.161–185.

González-Montellano, C., Fuentes, J.M., Ayuga-Téllez, E., Ayuga, F., 2012. Determination of the mechanical properties of maize grains and olives required for use in DEM simulations. *Journal of Food Engineering*, 111, pp.553–562.

Govender, I., Cleary, P.W., Mainza, A.N., 2013. Comparisons of PEPT derived charge features in wet milling environments with a friction-adjusted DEM model. *Chemical Engineering Science*, 97, pp.162–175.

Govender, I., Powell, M.S., Nurick, G.N., 2001. 3D particle tracking in a mill: A rigorous technique for verifying DEM predictions. *Minerals Engineering*, 14(10), pp.1329–1340.

Gupta, A., Yan, D.S., 2006. *Mineral Processing Design and Operation*, Elsevier.

Gustafsson, G., Häggblad, H.A., Jonsén, P., 2013. Multi-particle finite element modelling of the compression of iron ore pellets with statistically distributed geometric and material data. *Powder Technology*, 239, pp.231–238.

HBM, 2012. T20WN Torque Transducer data sheet. *Hottinger Baldwin Messtechnik (HBM)*.

Jaeger, H.M., Nagel, S.R., 1992. Physics of the granular state. *Science*, 255(5051), pp.1523–1531.

Johnson, K.L., 1985. *Contact Mechanics*, Cambridge University Press.

Khanal, M., Morrison, R.D., 2008. Discrete element method study of abrasion. *Minerals Engineering*, 21(11), pp.751–760.

Kiangi, K., Potapov, A., Moys, M.H., 2013. DEM validation of media shape effects on the load behaviour and power in a dry pilot mill. *Minerals Engineering*, 46-47, pp.52–59.

King, R.P., 2001. *Modelling & Simulation of Mineral Processing Systems*, Oxford: Butterworth-Heinemann.

Mayank, K., Malabe, M., Govender, I., Mangadoddy, N., 2015. Coupled DEM-CFD Model to Predict the Tumbling Mill Dynamics. *Procedia IUTAM*, 15, pp.139–149.

Mindlin, R.D., 1949. Compliance of elastic bodies in contact. *Journal of Applied Mechanics*, (16), pp.259–268.

Mishra, B.K., 2003. A review of computer simulation of tumbling mills by the discrete element method: Part I - contact mechanics. *International Journal of Mineral Processing*, 71, pp.73–93.

Mishra, B.K., Rajamani, R.K., 1992. The discrete element method for the simulation of ball mills. *Applied Mathematical Modelling*, 16(April), pp.598–604.

Misra, A., Cheung, J., 1999. Particle motion and energy distribution in tumbling ball mills. *Powder Technology*, 105(1-3), pp.222–227.

Montgomery, D.C., 2013. Design and Analysis of Experiments.

Morrel, S., 1996. Power draw of wet tumbling mills and its relationship to charge

dynamics - Part 1: a continuum approach to mathematical modelling of mill power draw. *Transactions of the Institute of Mining and Metallurgy*, 105(Section C), pp.43–53.

Mudd, G.M., 2010. The Environmental sustainability of mining in Australia: key mega-trends and looming constraints. *Resources Policy*, 35(2), pp.98–115.

van Nierop, M.A., Glover, G., Hinde, A.L., Moys, M.H., 2001. A discrete element method investigation of the charge motion and power draw of an experimental two-dimensional mill. *International Journal of Mineral Processing*, 61(2), pp.77–92.

Norgate, T., Jahanshahi, S., 2011. Reducing the greenhouse gas footprint of primary metal production: Where should the focus be? *Minerals Engineering*, 24(14), pp.1563–1570.

Oliveira, C.R., Werlang, T., 2007. Ergodic hypothesis in classical statistical mechanics. *Revista Brasileira de Ensino de Física*, 29(2), pp.189–201.

Parker, D.J., Hawkesworth, M.R., Broadbent, C.J., Fowles, P., Fryer, T.D., McNeil, P.A., 1994. Industrial positron-based imaging : principles and applications. *Nuclear Instruments and Methods in Physics Research Section A*, 348, pp.583–592.

Parker, D.J., Broadbent, C.J., Fowles, P., Hawkesworth, M.R., McNeil, P., 1993. Positron emission particle tracking - a technique for studying flow within engineering equipment. *Nuclear Instruments and Methods in Physics Research Section A: Accelerators, Spectrometers, Detectors and Associated Equipment*, 326, pp.592–607.

Parker, D.J., Dijkstra, A.E., Martin, T.W., Seville, J.P.K., 1997. Positron emission particle tracking studies of spherical particle motion in rotating drums. *Chemical Engineering Science*, 52(13), pp.2011–2022.

Parker, D.J., Forster, R.N., Fowles, P., Takhar, P.S., 2002. Positron emission particle tracking using the new Birmingham positron camera. *Nuclear Instruments and Methods in Physics Research Section A: Accelerators, Spectrometers, Detectors and Associated Equipment*, 477(1-3), pp.540–545.

Parker, D.J., Fan, X., 2008. Positron emission particle tracking—Application and labelling techniques. *Particuology*, 6(1), pp.16–23.

Pérez-Alonso, C., Delgadillo, J.A., 2012. Experimental validation of 2D DEM code by digital image analysis in tumbling mills. *Minerals Engineering*, 25(1), pp.20–27.

Powell, M.S., McBride, A.T., 2004. A three-dimensional analysis of media motion and grinding regions in mills. *Minerals Engineering*, 17(11-12), pp.1099–1109.

Powell, M.S., Nurick, G.N., 1996. A study of charge in rotary mills Part 3 - Analysis of results. *Mineral Engineering*, 9(4), pp.399–418.

Sichalwe, K., Govender, I., Mainza, A.N., 2011. Characterising porosity of multi-

component mixtures in rotary mills. *Minerals Engineering*, 24(3-4), pp.276–281.

Tavares, L.M., Carvalho, R.M., 2010. A Mechanistic Model of Batch Grinding in. *XXV International Mineral Processing Congress (IMPC)* 2010, pp.1287–1297.

Torquato, S., Truskett, T.M., Debenedetti, P.G., 2000. Is Random Close Packing of Spheres Well Defined? *Physical Review Letters*, 84(10), pp.2064–2067.

Venugopal, R., Rajamani, R.K., 2001. 3D simulation of charge motion in tumbling mills by the discrete element method. *Powder Technology*, 115(2), pp.157–166.

Weerasekara, N, Powell, M., Cleary, P., Tavares, L.M., Evertsson, M., Morrison, R., Quist, J., Carvalho, R., 2013. The contribution of DEM to the science of comminution. *Powder Technology*, 248, pp.3–4.

Wills, B.A. & Napier-Munn, T., 2006. *Mineral Processing Technology* (*Seventh Ed.*), Butterworth-Heinemann.

Yang, R.Y., Zou, R.P., Yu, A.B., 2003. Microdynamic analysis of particle flow in a horizontal rotating drum. *Powder Technology*, 130, pp.138–146.